Chaos, Solitons and Fractals 159 (2022) 112188

Contents lists available at ScienceDirect

Chaos, Solitons and Fractals

Nonlinear Science, and Nonequilibrium and Complex Phenomena

journal homepage: www.elsevier.com/locate/chaos

Controlling chaotic oscillations in a symmetric two-mass model of the vocal folds

Oriol Guasch [a,*], Annemie Van Hirtum [b], A. Inés Fernández [c], Marc Arnela [a]

[a] Department of Engineering, La Salle, Universitat Ramon Llull, C/Quatre Camins 30, 08022 Barcelona, Catalonia, Spain
[b] Univ. Grenoble Alpes, CNRS, Grenoble INP, LEGI, 38000 Grenoble, France
[c] Department of Materials Science and Physical Chemistry, University of Barcelona, Catalonia, Spain

ARTICLE INFO

Article history:
Received 23 November 2021
Received in revised form 22 April 2022
Accepted 2 May 2022
Available online xxxx

Keywords:
Vocal fold pacemaker
Vocal fold dynamics
Chaotic self-oscillations
Chaos control
Smart materials
Two-mass models

ABSTRACT

Human phonation is a highly non-linear process in which subglottal flow emanating from the lungs induces self-oscillations of the vocal folds. In normal conditions, this results in the generation of a regularly pulsating volume velocity that becomes the source of acoustic waves, which once modulated by the vocal tract, get emitted outwards as voice. However, vocal fold oscillations can become chaotic under many circumstances. For instance, even in the case of healthy symmetric vocal folds, an excess value of the subglottal pressure can trigger chaotic motion. In this paper, we derive a chaos control strategy for a two-mass model of the vocal cords to revert the situation and render the motion regular again. The approach relies on slightly altering the system energy to move it to a stable state. Given that no external control forces can be applied to the vocal cords, it is proposed to add a third mass to the original two-mass model, which is assumed to be made of an ideal smart material. The mass of the smart material is presumed negligible in comparison to the two masses of the vocal folds model, but its damping and stiffness can be tuned to evolve with time. For a fixed subglottal pressure for which the motion is chaotic, it is shown how periodicity can be recovered using adequate damping laws, by either attaching the smart material onto the larger vocal fold mass or onto the smaller one. For the latter, chaos control turns to be more difficult and the damping of the smart material has to quickly vary with time. On the other hand, given that the subglottal pressure would rarely be constant in a real situation, we also introduce a damping law to avoid chaotic motion as the subglottal pressure augments or diminishes. Finally, it is shown that control can not only be achieved by acting on the damping of the smart material but also on its stiffness. A stiffness law to prevent chaotic oscillations and get a healthy pulsating volume velocity is therefore implemented. A brief discussion on the mid-long term potential of the presented solution for practical cases is included.

1. Introduction

The essentials of the myoelastic aerodynamic theory of human phonation are nowadays well understood [1,2]. In a nutshell, the air emanating from the lungs reaches the larynx and exerts a pressure on the vocal folds which open once surpassed a certain threshold value. This opening causes the pressure to suddenly drop and as a consequence the vocal folds close again until the subglottal pressure becomes strong enough to force a new aperture. In this way, self-oscillations of the vocal folds are established. The regular opening/closing of the vocal cords results in a glottal volume velocity that acts as a source term of acoustic waves. The latter propagate and become modulated inside the vocal tract and get finally emitted outside the mouth, as voice.

The process of phonation is highly non-linear due to the complex combination of non-linear biomechanics involving impacts and aerodynamics, and can often lead to chaotic oscillations of the vocal folds, which may induce abnormal and unpleasant voice. This is often the case in voice pathologies like unilateral paralyses or in lesions involving nodules, polyps or cysts. To better understand the physics behind those phenomena, several low-dimensional models of the vocal folds were developed during the past half century, consisting of mass-spring-damper systems driven by glottal flow excitation. The investigation on the so-called mass models began in the earlier seventies, being probably the two-mass model of Ishizaka and Flanagan the most celebrated one [3]. However, it was not until the nineties that non-linear dynamics methods were used to understand the bifurcation processes that led from regular vocal fold motion to chaotic one (see e.g., [4–6]). Investigations on lumped mass models of increasing complexity [7–10] continued through the next decades and low dimensional models for the vocal fold self-oscillations [11–13] and glottal flows [14,15] still

* Corresponding author.
E-mail address: oriol.guasch@salle.url.edu (O. Guasch).

https://doi.org/10.1016/j.chaos.2022.112188

constitute a very active area of experimental and theoretical research. In fact, it would be interesting to check whether advances and new proposals in the classification of attractors and bifurcation theory [16], like the identification of hidden attractors [17–19] and/or hyperchaos [20–22] could be of relevance for some of these lumped models of the vocal folds and if they could have physical implications in terms of voice production.

Despite all efforts made to understand the physical mechanisms of voice disorders, the possibility of establishing control strategies that could revert chaotic vocal fold vibrations to regular ones have not been explored yet. The main novelty of this paper is to examine if that could be feasible or not. To the best of our knowledge this has not been attempted before. Using low dimensional mass models, we aim at a theoretical design of a vocal fold pacemaker that could improve voice quality. It is to be noted that laryngeal pacemakers have been among us for decades [23–25] and recent progress have been achieved on them [26–28]. However, such pacemakers are not intended at all to deal with voice generation problems but are designed to solve critical medical problems related to abduction and inspiration.

In this paper we will make use of the two-mass model in [5] and propose a control approach for chaotic vocal fold oscillations. To facilitate the analysis we will deal with the easiest case in which the two-mass model is totally symmetric, i.e. there are no geometrical or physical differences between the left and right vocal cords. It was shown in [29] that even in this simple situation chaotic motion could arise for high enough subglottal pressure values. This results in irregular glottal volume velocity and, therefore, in poor voice quality. There exist several feedback chaos control schemes that are useful for non-linear mechanical systems involving impacts, like the ones we encounter in the modeling of the vocal folds. The popular Ott-Grebogi-Yorke (OGY) strategy [30] essentially locates an unstable periodic orbit embedded in a chaotic attractor and then stabilizes the orbit by inducing small perturbations on a control parameter. The OGY method has been successfully applied to a large variety of problems and it performs well in those with impacts, see e.g. [31]. On the other hand, since the proposal of delayed feedback control strategies in [32,33] a vast amount of feedback control algorithms have been successfully developed (see e.g., the reviews in [34–36]), which have also turned to be very efficient in stabilizing a large variety of mechanical problems that include contact [37–40]. More recently, another feedback strategy was suggested which does not require knowing the system equations and basically relies on its output time series [41,42]. The basic idea in [41,42] is to slightly alter the time averaged oscillation energy (kinetic plus potential) of the system to move it to a value where it becomes stable. Such approach has proved valid for classical non-linear oscillators (e.g., Van der Pol and Duffing oscillators), for networks of oscillators, and for colliding elements as well [43]. Given that our two-mass model driven by the glottal flow involves more than one mass and also deals with contact between vocal folds, we have relied on the strategy in [41,42] to help transitioning the chaotic motion of the vocal folds to periodic one, and get an appropriate glottal volume velocity. It is to be remarked that the volume velocity will be our variable of primary interest throughout the paper.

The main novel contributions of this work are as follows. First, let us note that most chaos controlling approaches, like that in [41,42], depend on applying an external control force to stabilize the system. Given that this would not be possible in the case of the vocal folds, our proposal is to substitute that force by the inclusion of a third mass, made of a smart material, in the original two-mass model of the vocal folds. The smart material is assumed to be ideal in the sense of its mass being negligible in comparison to the lower large mass and upper small mass of the vocal folds model, and also in the sense of having the property that its damping and stiffness can be tuned to evolve with time without restrictions. In some way, the suggested strategy corresponds to swapping the external control force from the right hand side of the system of equations to the left hand side, and integrate it as an internal force with variable parameters. After establishing the new model, we propose different laws for reverting the vocal cords motion from chaotic to periodic. For a fixed subglottal pressure value, if one attaches the smart material to the large mass of the vocal folds it suffices to increase the overall damping value to transition to a stable state. However, achieving control by gluing the smart material to the small mass is by far more subtle and the time evolving law in [41,42] becomes necessary to get a robust solution, in which the vocal folds still collide closing the glottis. On the other hand, given that in practice the subglottal pressure that drives the vocal cord self-oscillations will not be constant, we introduce a new feedback mechanism to guarantee a periodic volume velocity in such situation. Finally, we show that chaos control can not only be achieved by modifying the damping of the smart material but also by changing its stiffness. An appropriate law is introduced to do so.

The paper is organized as follows. In Section 2, we present the ODE system corresponding to the symmetric two-mass model in [5,29]. Section 3 contains a brief review of the performance of that model when varying the subglottal pressure and the contact stiffness between masses. Special emphasis is placed on the consequences for the glottal volume velocity when transitioning to chaotic motion. In Section 4, we start reviewing the control strategy in [41,42] and then propose the idea of applying it to our problem by including a third smart material mass into the system. The section continues by exploring several damping laws to either control the large mass or the small mass of the system and analyzes the impact that this has on the volume velocity. Then, the case of non-constant subglottal pressure is addressed and a chaos control approach is derived for it. Finally, it is shown that stabilization can also be achieved by modifying the stiffness of the smart material. A short discussion follows considering the mid-long term potential of the proposed theoretical solution based on currently existing smart materials and their properties [44]. The conclusions close the paper in Section 5.

2. Non-linear ODE system for the symmetric vocal fold two-mass model

Through years, several models have been proposed to simulate the underlying physics of phonation and in particular the onset of self-oscillations of the vocal folds. The latter are located in the larynx, which connects the trachea and the vocal tract, and can be mechanically represented as a distributed system of masses, springs and dampers. The glottis is the opening between vocal folds. The easiest models that are able to reproduce the essential physiological and mechanical properties of phonation, namely the interaction between the vocal fold geometry and the glottal airflow obeying Bernouilli's equation are the two-mass models [3]. In such models, a vocal cord is separated in depth (thickness) into an upper and lower part, each one consisting of an oscillator characterized by mass, stiffness and damping values (see Fig. 1). If one considers the case of symmetric vocal folds, it suffices to study the dynamics of either the right or left ones. The latter have been chosen in this work. The phase lag between the lower and upper masses m_{1l} and m_{2l} in Fig. 1 is essential for the generation of self-sustained oscillations, which can not be reproduced by single mass models.

Assuming that the cubic nonlinearity of the oscillators in the Ishizaka and Flanagan two-mass model is small, that the interaction of the vocal folds and glottal flow dynamics are independent of subglottal and supraglottal resonances in the trachea and vocal tract, and that the approximation of Bernouilli's flow applies, the equations of motion for m_{1l} and m_{2l} can be derived from Newton's second law (see e.g., [5,29] for more details),

$$m_{1l}\ddot{x}_{1l} + r_{1l}\dot{x}_{1l} + k_{1l}x_{1l} + k_{cl}(x_{1l} - x_{2l}) + \Theta(-a_1)c_{1l}\frac{a_1}{2L} = P_1 L d_{1l}, \tag{1a}$$

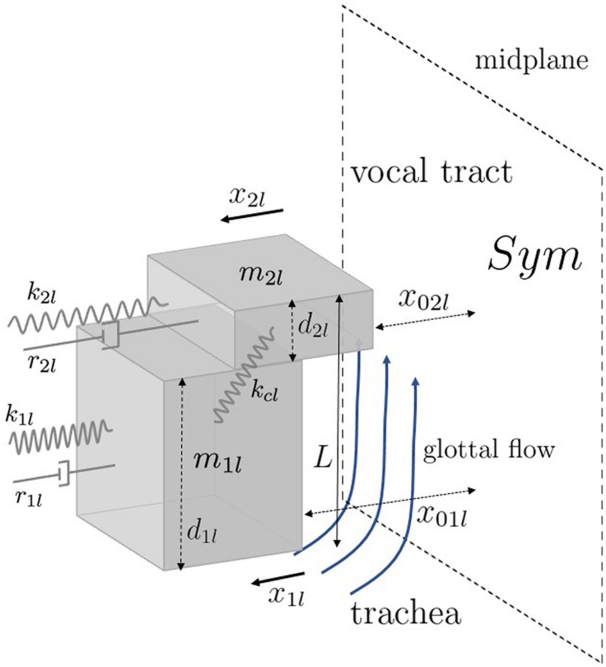

Fig. 1. Schematic representation of the two-mass model of the vocal folds described by Eq. (4). As we are considering the symmetric case, only the left vocal cords and its associated variables and parameters are represented.

$$m_{2l}\ddot{x}_{2l} + r_{2l}\dot{x}_{2l} + k_{2l}x_{2l} + k_{cl}(x_{2l} - x_{1l}) + \Theta(-a_2)c_{2l}\frac{a_2}{2L} = 0, \tag{1b}$$

where, r_{il} $(i = 1, 2)$ stand for the damping constants, k_{il} $(i = 1, 2)$ for the stiffness ones and k_{cl} is the coupling stiffness between the upper and lower masses (see Fig. 1). The dampers r_{il} account for the mass stickiness when the moist surfaces of the left and right vocal folds do have contact [3]. The springs with stiffness k_{il} are a representation of the tension of the vocal folds, which is controlled by the contraction of the anterior cricothyroid muscle, among others [2,3]. In what concerns the coupling stiffness, k_{cl}, it characterizes the flexural stiffness in the lateral direction of the vocal cords. Likewise, the fifth term on the left hand side (l.h.s) of Eqs. (1a) and (1b) is the non-linear collision force between the right and left vocal folds. $a_i = a_{0i} + 2Lx_{il}$ $(i = 1,2)$ are the lower and upper glottal areas with L being the length of the glottis and $a_{0i} = 2Lx_{0il}$ (i = 1,2) the lower and upper glottal rest areas (x_{0il} stands for the distance of m_{il} to the midline in the rest position). The collision function Θ is approximated by $\Theta(z) = \tanh(50z/z_0)$ for $z>0$ and becomes zero if $z \leq 0$. z_0 is taken as a_{01} in the computations. $c_{il}(i = 1, 2)$ are additional spring constants during collision. As regards the force term in the right hand side (r.h.s) of Eq. (1a), d_{1l} is the thickness of m_{1l} and P_1 is the glottal pressure acting on it. Bernoulli's equation allows one to derive the following expression for P_1,

$$P_1 = P_s\left[1 - \Theta(a_{\min})\left(\frac{a_{\min}}{a_1}\right)^2\right]\Theta(a_1), \tag{2}$$

with P_s being the subglottal pressure and $a_{\min} = a_1$ if $x_{1l} < x_{2l}$ while $a_{\min} = a_2$ if $x_{2l} \leq x_{1l}$.

An important parameter for voice generation is the volume flow velocity, U. This acts as a source term which excites acoustic waves in the vocal tract that become radiated as voice outside the mouth. U is typically prescribed as a boundary condition at the glottis in numerical voice production studies (see e.g., [45–48]). The volume flow velocity can be computed as,

$$U = \left(\frac{2P_s}{\rho}\right)^{1/2} a_{\min}\Theta(a_{\min}). \tag{3}$$

Eqs. (1a) and (1b) can be converted into a first-order non-linear ODE system of the type $\dot{y} = A(y)y + f(y)$ by introducing the mass velocities $v_{1l} = \dot{x}_{1l}$ and $v_{2l} = \dot{x}_{2l}$ as independent variables. This yields,

$$\begin{aligned}\dot{\mathbf{y}} \equiv \begin{pmatrix}\dot{\boldsymbol{v}}\\ \dot{\boldsymbol{x}}\end{pmatrix} &= \begin{pmatrix}-\mathbf{M}^{-1}\mathbf{C} & -\mathbf{M}^{-1}(\mathbf{K}+\boldsymbol{\Theta}(\boldsymbol{x}))\\ \mathbf{I} & \mathbf{0}\end{pmatrix}\begin{pmatrix}\boldsymbol{v}\\ \mathbf{x}\end{pmatrix} + \begin{pmatrix}\mathbf{M}^{-1}\boldsymbol{f_v}(\boldsymbol{x})\\ \mathbf{0}\end{pmatrix}\\ &\equiv \mathbf{A}(\boldsymbol{y})\boldsymbol{y} + f(\boldsymbol{y}) \equiv g(\boldsymbol{y}),\end{aligned} \tag{4}$$

where $\boldsymbol{v} = (v_{1l}, v_{2l})^\top$ is the mass velocity vector and $\boldsymbol{x} = (x_{1l}, x_{2l})^\top$ the displacement one, so that $\boldsymbol{y} = (\boldsymbol{v}, \boldsymbol{x})^\top$, as identified in Eq. (4). The force vector component is given by $\boldsymbol{f_v} = (P_1Ld_{1l}, 0)^\top$. It is also common to express Eq. (4) as $\dot{\boldsymbol{y}} = g(\boldsymbol{y})$, with $g(\boldsymbol{y}) = A(\boldsymbol{y})\boldsymbol{y} + f(\boldsymbol{y})$, as shown in the last equality of Eq. (4). The block matrices in $\mathbf{A}$ correspond to the identity $\mathbf{I}$, and to the mass, $\mathbf{M}$, damping, $\mathbf{C}$, stiffness, $\mathbf{K}$ and collision, Θ, matrices given by,

$$\begin{aligned}&\mathbf{M} = \operatorname{diag}(m_{1l}, m_{2l}), \qquad \mathbf{C} = \operatorname{diag}(r_{1l}, r_{2l}),\\ &\mathbf{K} = \begin{pmatrix}k_{1l}+k_{cl} & -k_{cl}\\ -k_{cl} & k_{2l}+k_{cl}\end{pmatrix} \quad \Theta = \operatorname{diag}\left(\Theta(-a_1)c_{1l}\left[\frac{a_{01}}{2Lx_{1l}}+1\right], \Theta(-a_2)c_{2l}\left[\frac{a_{02}}{2Lx_{2l}}+1\right]\right).\end{aligned} \tag{5}$$

Note that the non-linearity enters the ODE system through $\boldsymbol{\Theta}(\boldsymbol{x})$ and $\boldsymbol{f_v}(x)$. The dynamics of Eq. (4) has been analyzed at extent in [5,29], showing that for slightly higher values of the coupling constant k_{cl} than usual, and for large subglottal pressure values, P_s, the motion of the two vocal fold masses can become aperiodic, or even chaotic. We will briefly review some of these aspects in the following section. It is to be noted that such abnormal behaviour of the vocal folds can have a profound impact on the glottal volume flow velocity U, and therefore, in the quality of the generated voice.

3. Chaotic motion of the vocal folds at high subglottal pressure and effects on the glottal volume flow velocity

For subsequent simulations, the physical and geometrical parameters in Table 1 have been employed. Throughout this text, the dimensions of the various variables will not be written (though they will be explicitly indicated in figures). They correspond to appropriate combinations of taking the following dimensions for length $[L] = $ cm, time $[T] = $ ms and mass $[M] = $ g. It is to be noted that the standard value for the coupling stiffness of $k_{cl} = 0.025$ has been increased to $k_{cl} = 0.09$ in the simulations following [29]. As said, the system in Eq. (4) was studied in detail in the past. Its dynamic behaviour dependence on the values of various model parameters was investigated and standard methods of non-linear analysis were applied to it. In [5], the existence and stability of fixed points was addressed through linearisation, while in [29] a combination of techniques were used to

Table 1
Physical and geometrical parameters of the vocal folds (see [5,29]).

Physical parameters	Geometry parameters
$m_{1l} = 2.5\,\mathrm{g}$	$d_{1l} = 0.25\,\mathrm{cm}$
$m_{2l} = 0.125\,\mathrm{g}$	$d_{2l} = 0.05\,\mathrm{cm}$
$r_{1l} = 0.02\,\mathrm{g\,ms^{-1}}$	$L = 1.4\,\mathrm{cm}$
$r_{2l} = 0.01\,\mathrm{g\,ms^{-1}}$	$a_{01} = 0.05\,\mathrm{cm^2}$
$k_{1l} = 0.08\,\mathrm{g\,ms^{-2}}$	$a_{02} = 0.05\,\mathrm{cm^2}$
$k_{2l} = 0.008\,\mathrm{g\,ms^{-2}}$	
$k_{cl} = 0.09\,\mathrm{g\,ms^{-2}}$	
$c_{1l} = 3k_{1l}\,\mathrm{g\,ms^{-2}}$	
$c_{2l} = 3k_{2l}\,\mathrm{g\,ms^{-2}}$	
$\rho = 0.00113\,\mathrm{g\,cm^{-3}}$	

discriminate under which conditions the motion of the masses becomes chaotic. The authors found that the system exhibits one positive Lyapunov exponent for large enough subglottal pressure values, which proves the existence of chaos (a Kaplan-Yorke dimension of 2.4 was reported indicating low-dimensional chaos). Despite being four dimensional, hyperchaos is therefore not possible in this particular system because at least two positive Lyapunov exponents are necessary for that to occur (see e.g. [20–22]). Strange attractors at the phase spaces of the two masses were reported in [29], as well as broadband noisy spectra and complex Poincaré sections. Bifurcation plots for the mass displacement amplitudes in terms of k_{cl}, P_s and further parameters were shown pointing out to a period doubling route to chaos.

In this section, we will only outline the essentials of the behaviour of the system in Eq. (4) in a nutshell. The interested reader is referred to the original works [5,29] for details. In contrast to the general approach in [5,29], however, special emphasis will be placed herein on the effects that the vocal fold dynamics have on the volume velocity U. All simulations in this work have been carried out implementing a standard fourth-order Runge-Kutta numerical method.

One can basically distinguish three different regimes for the vocal folds motion when we fix all system parameters but progressively increase the subglottal pressure P_s. These are captured in Fig. 2, where we plot different type of results for $P_s = \{0.0035, 0.021, 0.036\}$. Each row in the figure corresponds to a value of P_s that is representative of

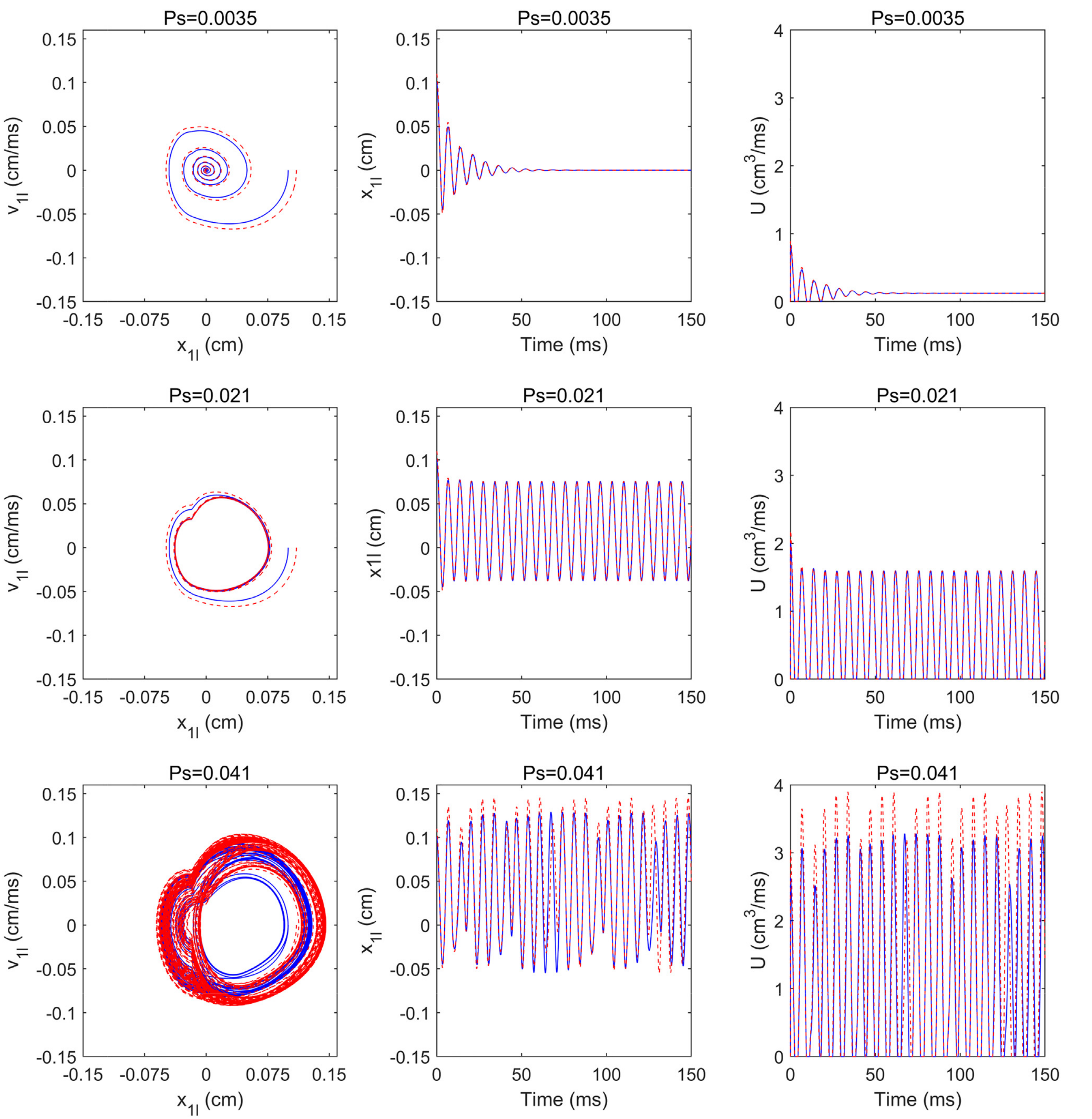

Fig. 2. Vocal fold dynamics for different values of the subglottal pressure P_s. Blue line: set of initial conditions $y_1(0)$. Red dashed line: set of initial conditions $y_2(0)$. Left column: phase space plot of v_{1l} versus x_{1l} for mass m_{1l}. Mid column: time evolution of the position x_{1l} of m_{1l}. Right column: time evolution of the glottal volume flow velocity. (For interpretation of the references to colour in this figure legend, the reader is referred to the web version of this article.)

such regimes. The first column contains trajectories in the phase space for m_{1l}, the second column shows the time evolution of x_{1l} and the third one plots the time evolution of U. The results for m_{2l} are very similar to those of m_{1l} and add no physical insight into the problem. Consequently they have not been included for the sake of brevity. The blue lines in the figure have been obtained from the solution of Eq. (4) using the set of initial conditions $y_1(0) = (0,0,0.1,0.1)^\top$, while the red dashed ones correspond to the neighbouring initial condition $y_2(0) = (0,0,0.11,0.11)^\top$.

If we focus on the first row of the figure we observe that the pressure $P_s = 0.0035$ is unable to generate self-oscillations of the vocal folds. The trajectories in phase space are spirals that decay from the initial condition to the fixed point (0,0), i.e. the mass m_{1l} reaches the zero rest position where it stands still. Observe that the two spirals in the figure corresponding to the initial conditions $y_1(0)$ and $y_2(0)$ remain close to each other until they reach the origin. As regards the time evolution of x_{1l}, it shows a few oscillations until the mass stops. Again, the two lines in the figure remain very close one to each other but do not match. The glottal volume flow velocity U in the third subfigure of the first row becomes zero in a few occasions because of the impact between vocal folds, and then acquires a small residual constant value because the vocal folds do not contact in the rest position.

The situation in the second row would be the desirable one for voice generation (taking into account the very severe simplifications assumed in the model of Eq. (4)). When the subglottal pressure increases, at some point the solution exhibits a Hopf bifurcation and a limit cycle in phase space is formed. It can be observed in the first figure of the second row, that the two trajectories arising from $y_1(0)$ and $y_2(0)$ merge at the limit cycle and then oscillate with exactly the same time period (see the plot of x_{1l} versus time). The volume flow velocity is also periodic, as observed in the third figure of the second row. It remains zero during the vocal fold impacts, then increases to a maximum and then decreases again until the next impact occurs.

The conditions in the third row are the undesirable ones. As long as P_s grows, the system bifurcates again and the periodicity of the vocal fold self-oscillations is lost. For $P_s = 0.041$ the motion has already become chaotic, exhibiting a strong sensitivity to the initial conditions. This is apparent in the phase space plot, where strange attractors are observed and the trajectories starting from $y_1(0)$ and $y_2(0)$ quickly depart from each other. If we look at the plot of x_{1l} versus time, we also perceive that, after a few oscillations, the evolution of x_{1l} when starting at $y_1(0)$ clearly differs from that starting at $y_2(0)$. The motion is no longer periodic at all and exhibits sudden amplitude transitions. The same occurs for the volume flux velocity: neither the impacts nor the amplitudes of U are regular. Such circumstance could result in a severe loss of quality of the generated voice.

To better recognize the effects of the chaotic mass motion on the glottal volume flow velocity, U, in the first row of Fig. 3 we have taken advantage of Takens's theorem to recover the attractor in the phase space $\left(\dot{U}, U\right)$ by plotting $(U(t+\tau), U(t))$. Here, τ is a time lag. There are different options for choosing τ (e.g., one could take the first local minimum of the mutual information usually applied to determine the correlation dimension in time series analysis [49] c.f., [50]). For our purposes, a simpler option suffices. We have taken $\tau = 4T_{Ps=0.021} = 27.56$ with $T_{Ps=0.021}$ being the period of U when the pressure is $P_s = 0.021$ (see Fig. 2, second row, third column), which results in the blue line of the left-top subfigure in Fig. 3. Note that if we chose a different time delay, like $\tau = 20$, we get an homeomorphic result to the previous one (green line in the figure). However, when we increase the subglottal pressure to $P_s = 0.041$, a strange attractor develops in the phase space of U, as illustrated in the right-top plot of Fig. 3. While in the results of Fig. 2 the initial transients were included to show the dependence on initial conditions, Fig. 3 does not contemplate them. For completeness, in the bottom row of Fig. 3 we have plotted the value of U depending on the positions x_{1l} and x_{2l} of the two masses, namely $U(x_{1l}, x_{2l})$. The red colour indicates the values of x_{1l} and x_{2l} for which U equals zero, i.e. either the left first or second masses contact the right ones and no volume flow can pass through the glottis. The blue colour corresponds to positive values of U. The comparison between the two figures in the bottom row supports the information found from the attractors in the top row. Setting the subglottal pressure to $P_s = 0.041$ entails an abnormal, chaotic, behaviour of the motion of the masses and hence of U. Please note that different scales have been used for the left and right columns of Fig. 3 for better inspection, as increasing P_s from 0.021 to 0.041 implies a significant growth of the amplitude of the volume velocity.

Finally, and to complete this brief overview on the behaviour of the symmetric two-mass model, in Fig. 4 we have plotted bifurcation plots of the maximum amplitude displacements of m_{1l}, namely max $|x_{1l}|$, for two different situations. The left subfigure corresponds to fixing the subglottal pressure at $P_s = 0.041$ and then increasing the coupling stiffness constant from $k_{cl} = 0.025$ to $k_{cl} = 0.09$. As illustrated in the figure, for low values of k_{cl} the motion remains periodic but for k_{cl} close to 0.057 it becomes chaotic. Then, a window of aperiodic motion can be observed until the motion becomes chaotic again. In contrast, in the right subfigure we have kept $k_{cl} = 0.09$ fixed and changed the subglottal pressure from $P_s = 0.0001$ to $P_s = 0.08$. For small values of P_s, self-oscillations cannot be triggered and, as mentioned before, the masses stop after some initial transients. However, when the pressure overcomes a threshold value close to $P_s \approx 0.0056$, a Hopf bifurcation occurs and a limit cycle is established. The oscillations increase their amplitude as P_s augments, but once reached another limit value of $P_s \approx 0.0377$ they become chaotic. The right subfigure of Fig. 4 clearly exposes the process by which the three regimes previously shown in Fig. 2 develop.

Our goal in this paper is to determine whether it would be possible to establish some chaos controlling mechanism so that the results in the third row of Fig. 2 could look like those in the second row, and the phase space top-right subfigure in Fig. 3 for the volume flow velocity could be like the top-left one, even when the subglottal pressure is high. As said in the introduction of the paper, rather than trying to control the system by means of some external force, we aim to do so by attaching some kind of smart material to the vocal folds and modify their effective mechanical properties.

4. Controlling the chaotic motion of the vocal folds

4.1. Chaos control by altering the system energy through external forces

Let us next summarize the basics of the chaos control approach proposed in [41–43] and adapt it to the problem at hand. The key idea in those works is to either increase or lower the overall energy of the system to a value in which the system gets stabilized. For instance, if a change in a system parameter leads to a period-doubling bifurcation, its energy would typically grow as sub-harmonics would contribute to the fundamental frequency [41]. The sum of kinetic and potential energy of the vocal folds is given by

$$E = \frac{1}{2}\boldsymbol{v}^\top \mathbf{M}\boldsymbol{v} + \frac{1}{2}\boldsymbol{x}^\top \mathbf{K}\boldsymbol{x}, \tag{6}$$

which once averaged over time T becomes

$$<E> = \frac{1}{T}\int_0^T \left(\frac{1}{2}\boldsymbol{v}^\top \mathbf{M}\boldsymbol{v} + \frac{1}{2}\boldsymbol{x}^\top \mathbf{K}\boldsymbol{x}\right) dt. \tag{7}$$

If the system dynamics is periodic, T would correspond to its period, while if it is chaotic $T \to \infty$. The rate of energy change of the system is obtained from the time derivative of Eq. (6), taking into account that all involved block matrices in the first row of Eq. (4) are symmetric,

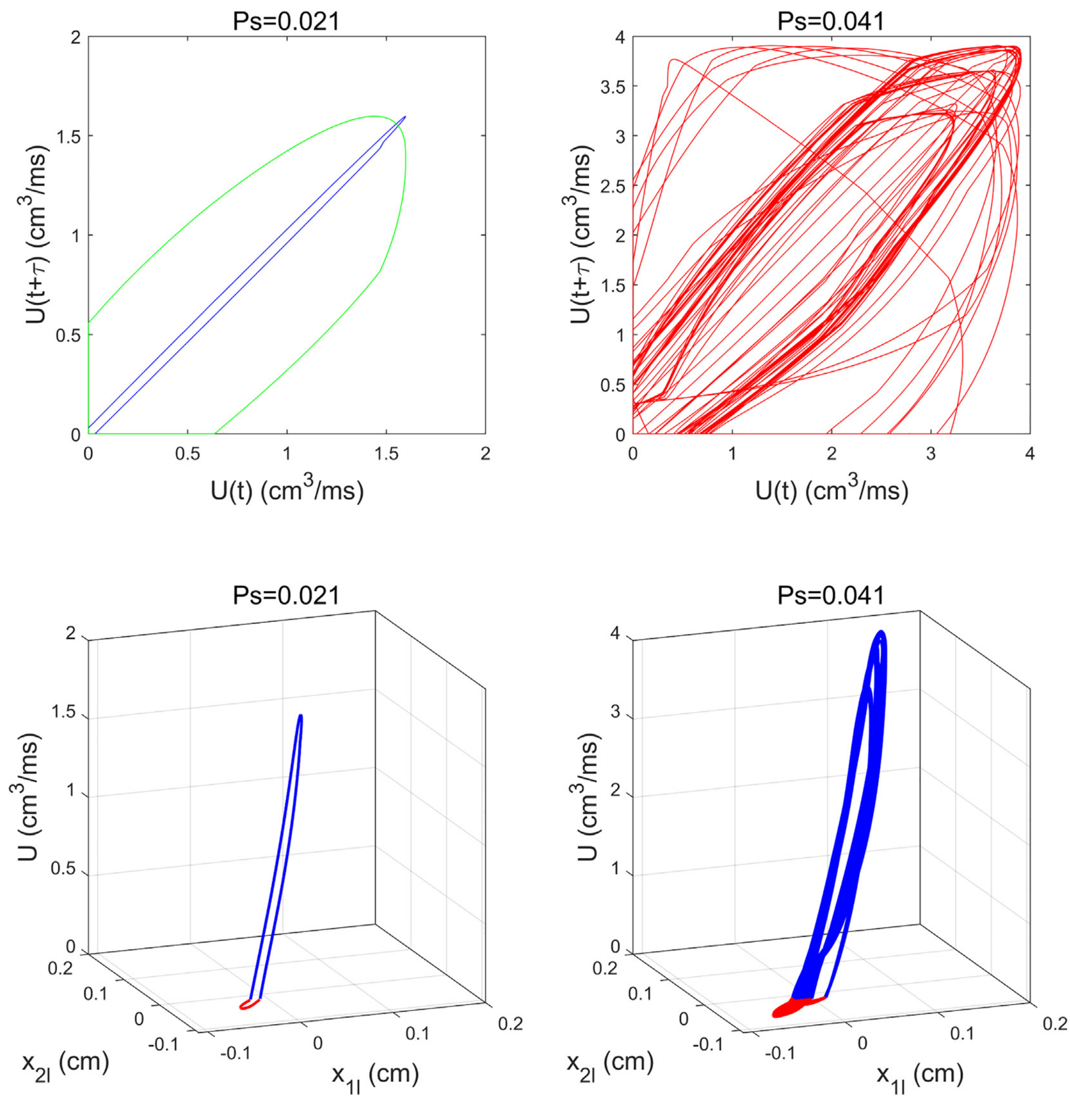

Fig. 3. First row: phase space plot for the glottal volume velocity $U(t+\tau)$ versus $U(t)$ for $P_s = 0.021$ and $P_s = 0.041$. Second row: volume velocity depending on the position of the two masses x_{1l} and $x_{2}l$, i.e., $U(x_{1l}, x_{2l})$. The red colour indicates zero values for U which occurs when the left and right masses do contact. Different scales have been used to better appreciate the difference between plots. (For interpretation of the references to colour in this figure legend, the reader is referred to the web version of this article.)

$$\dot{E} = \boldsymbol{v}^\top (\mathbf{M}\,\dot{\boldsymbol{v}} + \mathbf{K}\boldsymbol{x}) = \boldsymbol{v}^\top [-\mathbf{C}\boldsymbol{v} - \boldsymbol{\Theta}(\boldsymbol{x})\boldsymbol{x} + \boldsymbol{f}_{\mathbf{v}}(\boldsymbol{x})] \tag{8}$$

The control strategy in [41] essentially consists in adding a control force to Eq. (8) typically depending on the velocity and in some cases on position, namely $\boldsymbol{f}_c(\boldsymbol{v}, \boldsymbol{x})$, so that this equation becomes

$$\dot{E} = \boldsymbol{v}^\top (\mathbf{M}\,\dot{\boldsymbol{v}} + \mathbf{K}\boldsymbol{x}) = \boldsymbol{v}^\top [-\mathbf{C}\boldsymbol{v} - \boldsymbol{\Theta}(\boldsymbol{x})\boldsymbol{x} + \boldsymbol{f}_{\mathbf{v}}(\boldsymbol{x}) + \boldsymbol{f}_c(\boldsymbol{v}, \mathbf{x})], \tag{9}$$

and the control force is such that the power $\boldsymbol{v}^\top \boldsymbol{f_c}(\boldsymbol{v}, \boldsymbol{x})$ is either strictly positive or negative. This means that the control force will help increasing or decreasing the average system energy in Eq. (7), depending on the remaining non-linear components response to that change. The underlying idea is that the energy shift helps transitioning the system chaotic dynamics to periodic or quasiperiodic ones. Taking $\boldsymbol{f_c}(\boldsymbol{v})$, i.e., solely depending on the velocity $\boldsymbol{v}$ (typically a linear dependence suffices) has proved useful in stabilizing one dimensional non-linear systems like the Van der Pol and Duffing oscillators, as well as controlling systems with impact forces [41–43]. As said in the introduction of this manuscript, the strategy has also revealed efficient for the case of networks of oscillators with some non-linear terms [41,42]. Hence, one would expect the method to be effective for our vocal fold dynamics that involves two masses driven by flow pressure, which impact during their motion, closing the glottis. The option of taking $\boldsymbol{f_c}(\boldsymbol{x})$, i.e., a control force solely depending on the displacement $\boldsymbol{x}$ will be also considered in forthcoming sections, in addition to $\boldsymbol{f_c}(\boldsymbol{v})$. But, as explained before, instead of thinking about applying external control forces we will rather integrate them in the system and think in terms of attaching a smart material to the vocal folds whose intrinsic parameters can be modified.

4.2. Controlling the vocal folds with smart materials

In the case of the human vocal folds, adding an external control force $\boldsymbol{f_c}(\boldsymbol{v}, \boldsymbol{x})$ to the force vector $\boldsymbol{f_v}$ is not feasible. At most one could think of varying the vocal folds tension by stimulating the nerves driving them. As exposed in the introduction of the paper, this is at the basis of the few existent vocal fold pacemakers oriented at abduction and respiratory problems, but this approach would not work if the involved nerves were seriously damaged. The alternative we start exploring in this paper is whether it would be possible to control the

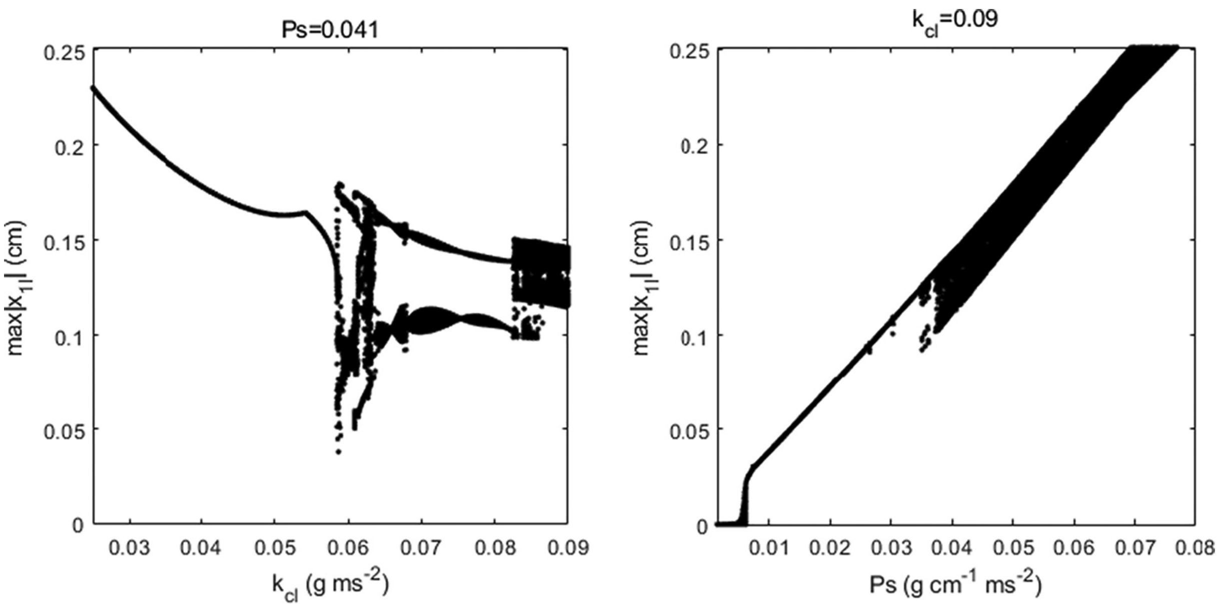

Fig. 4. Left subfigure: bifurcation plot for fixed $P_s = 0.041$ and varying stiffness coupling between masses from $k_{cl} = 0.025$ to $k_{cl} = 0.09$. Right subfigure: bifurcation plot for fixed $k_{cl} = 0.09$ and varying subglottal pressure from $P_s = 0.015$ to $P_s = 0.08$.

chaotic motion of the vocal folds by somehow attaching a smart material either to m_{1l} or to m_{2l}, such that its stiffness and/or damping could be modified at convenience. The situation is schematically depicted in Fig. 5, where in the left column the smart material is added to m_{1l}, while in the right column is glued to m_{2l}. The material has mass $m_{\rm sm}$ and will slightly elongate the glottis in a small quantity ΔL. Although these aspects could be easily incorporated in the model of Eq. (4), we will assume them negligible for simplicity in forthcoming simulations (i.e. we consider $m_{\rm sm} \ll m_{2l}, m_{1l}$ and $\Delta L \ll L$). The focus will be placed on finding appropriate laws for the varying smart material damping, $c_{il\rm con}(\boldsymbol{p}, t)$ and stiffness $k_{il\rm con}(\boldsymbol{p}, t)$, $i = 1, 2$, which may depend on variables $\boldsymbol{p} = \{\boldsymbol{x}, \boldsymbol{v}, U\}$ and time. As will be seen, most of the forthcoming work will concentrate on tuning the smart material damping to get an overall effective damping that suppresses the vocal folds chaotic motion. A final section on stiffness control will also be provided, though, as well as a brief discussion on the potential of current smart materials to attain our goal. Our exploration will be limited to the simple two-mass model in Eq. (4).

Instead of adding $\boldsymbol{f_c}(\boldsymbol{v}, \boldsymbol{x})$ to the force vector in Eq. (4), our smart material attempt is in fact equivalent to moving this term to the l.h.s of the equation so that the practical consequence is that of modifying the stiffness and/or damping matrices in $\mathbf{A}(\boldsymbol{y})$, by adding some control to them. In other words, we look for the effects of changing

$$\mathbf{C} \rightarrow \mathbf{C} + \mathbf{C}_c(\boldsymbol{v}, \boldsymbol{x}, U, t), \tag{10}$$

and/or

$$\mathbf{K} \rightarrow \mathbf{K} + \mathbf{K}_c(\boldsymbol{v}, \boldsymbol{x}, U, t), \tag{11}$$

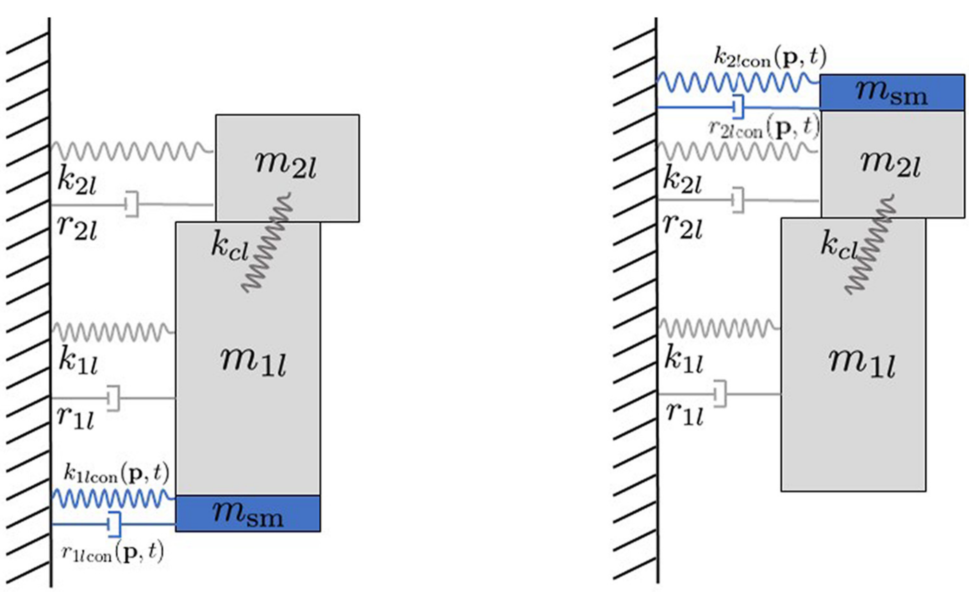

Fig. 5. Attaching a smart material to mass m_{1l} (left column) or to mass m_{2l} (right column). The damping $r_{il\rm con}(\boldsymbol{p}, t)$ and stiffness $k_{il\rm con}(\boldsymbol{p}, t)$ can depend on variables such as $\boldsymbol{p} = \{\boldsymbol{x}, \boldsymbol{v}, U\}$ and time, and be tuned so as to suppress the chaotic motion of the vocal folds.

where $\mathbf{C}_c$ and $\mathbf{K}_c$ refer to the damping and stiffness control matrices provided by the smart material. It is important to note here, that one does not need to alter all damping or stiffness entries in $\mathbf{C}$ and $\mathbf{K}$. The good news are that usually $\mathbf{C}_c$ and $\mathbf{K}_c$ will only have a single element different from zero. That is, modifying a single parameter suffices to stabilize the whole system. Before proceeding any further, it should be noticed that there is a trivial modification that could render the system stable. We know from the analysis in Section 3 that setting the coupling stiffness to $k_{cl} = 0.09$ instead of the standard value of $k_{cl} = 0.025$ (see [5,29]) triggers chaotic motion beyond a certain threshold subglottal pressure value. Recovering the value of $k_{cl} = 0.025$ would result in periodic motion of the vocal folds. Nevertheless, the challenge here is to see if that motion can be restored through other parameter modifications rather than k_{cl}.

4.2.1. Damping control

We start with one of the simplest possible options, which consists in altering the damping of the largest mass in the system, namely m_{1l}. This corresponds to taking a force $\boldsymbol{f}_c(\boldsymbol{v}) = \mathbf{C}_c\boldsymbol{v}$ that is integrated in the modified damping matrix of the system as follows,

$$\mathbf{C} = \mathrm{diag}(r_{1l}, r_{2l}) \rightarrow \mathbf{C} + \mathbf{C}_c = \mathrm{diag}(r_{1l} + r_{1l\mathrm{con}}, r_{2l}), \tag{12}$$

with $|r_{1l\mathrm{con}}| < |r_{1l}|$. Let us consider the case of a subglottal pressure of $P_s = 0.041$ like in the last row of Fig. 2 and take a small control value $r_{1l\mathrm{con}} = -0.1 r_{1l}$. Initially, we let the system evolve without control and when $t = 300$ we activate the new smaller damping. This results in a slight increase of the system average energy in Eq. (7), from $\langle E \rangle = 6.12 \times 10^{-4}$ to $\langle E_{\mathrm{con}} \rangle = 7.68 \times 10^{-4}$. The effects of diminishing the damping are plotted in Fig. 6. The first column in the figure corresponds to the results of the simulations without control, while the second column contains those with control. In the first row we observe how the strange attractor transforms to a cycle for the new damping value. The data in these figures have been plotted from $t = 500$ to $t = 1000$. In the second row it is seen how the displacement x_{1l} becomes periodic beyond $t = 300$, once the control is triggered. Also, the volume flow velocity in the third row becomes regular (compare it with the evolution of U in the last row of the first column), growing from zero, when the glottis is closed, to its maximum value and then decreasing again until the next contact between masses takes place. The time duration of the glottis closure remains constant when the control is activated. Very similar results are obtained for the mass m_{2l}

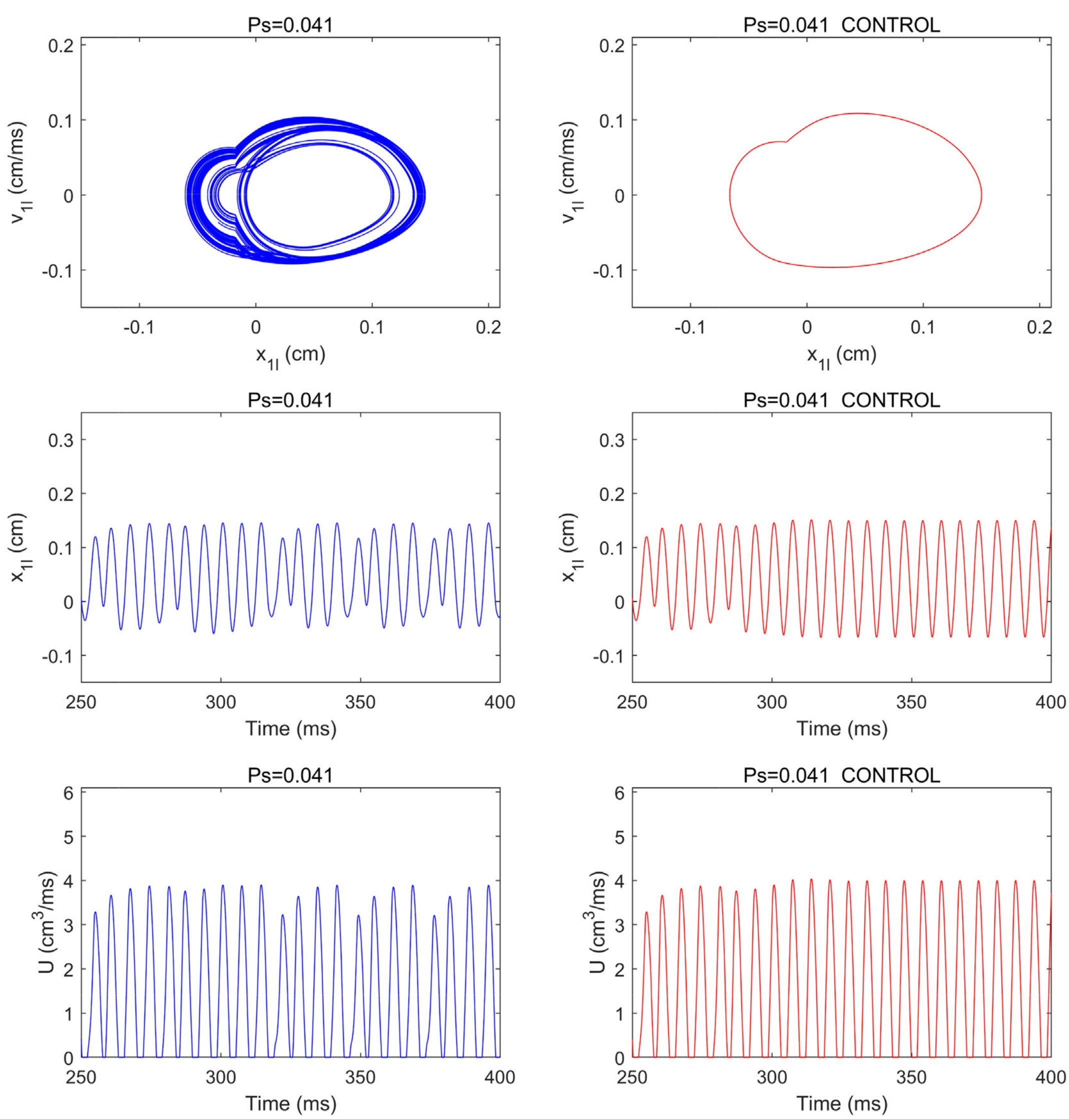

Fig. 6. Control by modifying the damping r_{1l} of mass m_{1l}. First column: system with no control. Second column: system with control. Damping activated at $t = 300$. First row: phase space attractor (v_{1l}, x_{1l}). Second row: time evolution of the displacement x_{1l}. Third column: time evolution of the glottal volume flow velocity. Results for a subglottal pressure of $P_s = 0.041$.

that will not be reproduced herein for brevity. To better appreciate the stabilization effects of decrementing the damping of m_{1l}, in the first row of Fig. 7 we have plotted the attractors in phase spaces (v_{1l}, x_{1l}) and (v_{2l}, x_{2l}) when no damping modification is applied (blue lines) and the closed orbits (red lines) achieved when $r_{1l\text{con}}$ is triggered. In the second row of the figure we make use again of Takens's theorem and plot $U(t+\tau)$ against $U(t)$ to show how the strange attractor in the left figure gets stabilized through damping in the right figure. The glottal flow volume velocity, which is our final most important variable for voice generation has therefore acquired the right shape.

Next, we may wonder what happens if instead of acting on the damping, r_{1l}, of the first mass, we act on r_{2l} of the second mass, m_{2l}. That is, we now make the modification,

$$\mathbf{C} = \text{diag}(r_{1l}, r_{2l}), \; \rightarrow \mathbf{C} + \mathbf{C}_c = \text{diag}(r_{1l}, r_{2l} + r_{2l\text{con}}), \tag{13}$$

with $|r_{2l\text{con}}| < |r_{2l}|$. The situation is now by far more tricky than when changing r_{1l}. The mass m_{2l} is twenty times smaller than m_{1l} and acting on it to control the whole dynamics of the system through r_{2l} is problematic. To begin with, testing $r_{2l\text{con}} = -0.1 r_{2l}$ is not enough to stabilize the system and a higher percentage of variation of r_{2l} is required. Periodicity is attained when $r_{2l\text{con}} \sim -0.25 r_{2l}$, but there is a problem associated to it. The time duration of the vocal folds contact is negligible and for slightly higher values of $r_{2l\text{con}}$, namely $\sim -0.29 r_{2l}$, it simply disappears. This means that while the glottal volume velocity U will be pulsating, it would never be zero, giving place to a breathy voice which is undesirable. The problem is clearly illustrated in Fig. 8 that shows equivalent subplots to the previous ones in Fig. 7. As observed in the first row, the motion of the two masses gets stabilized and two period-1 cycles clearly form. However, when we look at the volume velocity in the second row (bottom-right figure), it becomes apparent that its corresponding closed orbit does not cross the axes so the breathy effect will clearly manifest. In this case, the system average energy has decreased from $\langle E \rangle = 6.12 \times 10^{-4}$ to $\langle E_{\text{con}} \rangle = 5.9 \times 10^{-4}$. One may conclude that acting on the first vocal fold mass is clearly an easier way to get an acceptable glottal flow if damping changes are to be implemented (one could also consider changing both damping values simultaneously, though it would clearly be better to find a strategy involving as less control parameters as possible).

A more robust option than simply shifting r_{1l} or r_{2l} to new values is that of proposing a damping variation depending on the sign of the mass velocities. Following [41–43], we take

$$\mathbf{C} = \text{diag}(r_{1l}, r_{2l}) \rightarrow \mathbf{C} + \mathbf{C}_c = \text{diag}(r_{1l} + r_{1l\text{con}} \,\text{sgn}\,(v_{1l}), r_{2l}), \tag{14}$$

or, alternatively,

$$\mathbf{C} = \text{diag}(r_{1l}, r_{2l}) \rightarrow \mathbf{C} + \mathbf{C}_c = \text{diag}(r_{1l}, r_{2l} + r_{2l\text{con}} \,\text{sgn}\,(v_{2l})), \tag{15}$$

with $|r_{il\text{con}} \,\text{sgn}\,(v_{il})| < |r_{il}|$, $i = 1, 2$. This obviously implies that one should be able to change the damping of the smart material attached to the vocal folds very rapidly, at least twice per oscillation. This is a real challenge for current smart materials (see the discussion in Section 4.2.4). Here, the main difference with the previous proposals is that the amount of increased damping depends on the sign of the

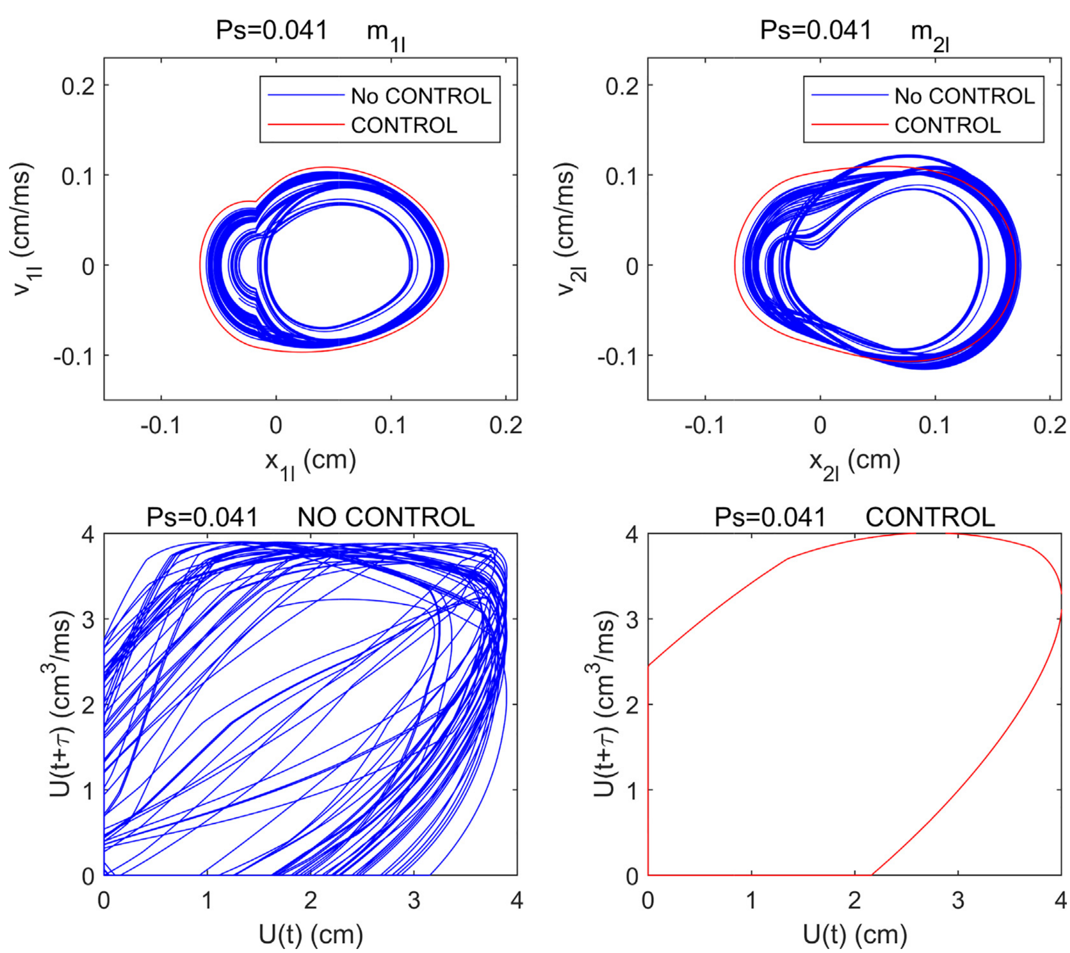

Fig. 7. First row: attractors and period-1 orbit for the system with (red) and without (blue) damping control $r_{1l\text{con}}$. Left: phase space (v_{1l}, x_{1l}), right: phase space (v_{2l}, x_{2l}). Second row: phase space plot for the glottal volume velocity $U(t+\tau)$ versus $U(t)$ without control (left) and with control (right). Results for a subglottal pressure of $P_s = 0.041$. (For interpretation of the references to colour in this figure legend, the reader is referred to the web version of this article.)

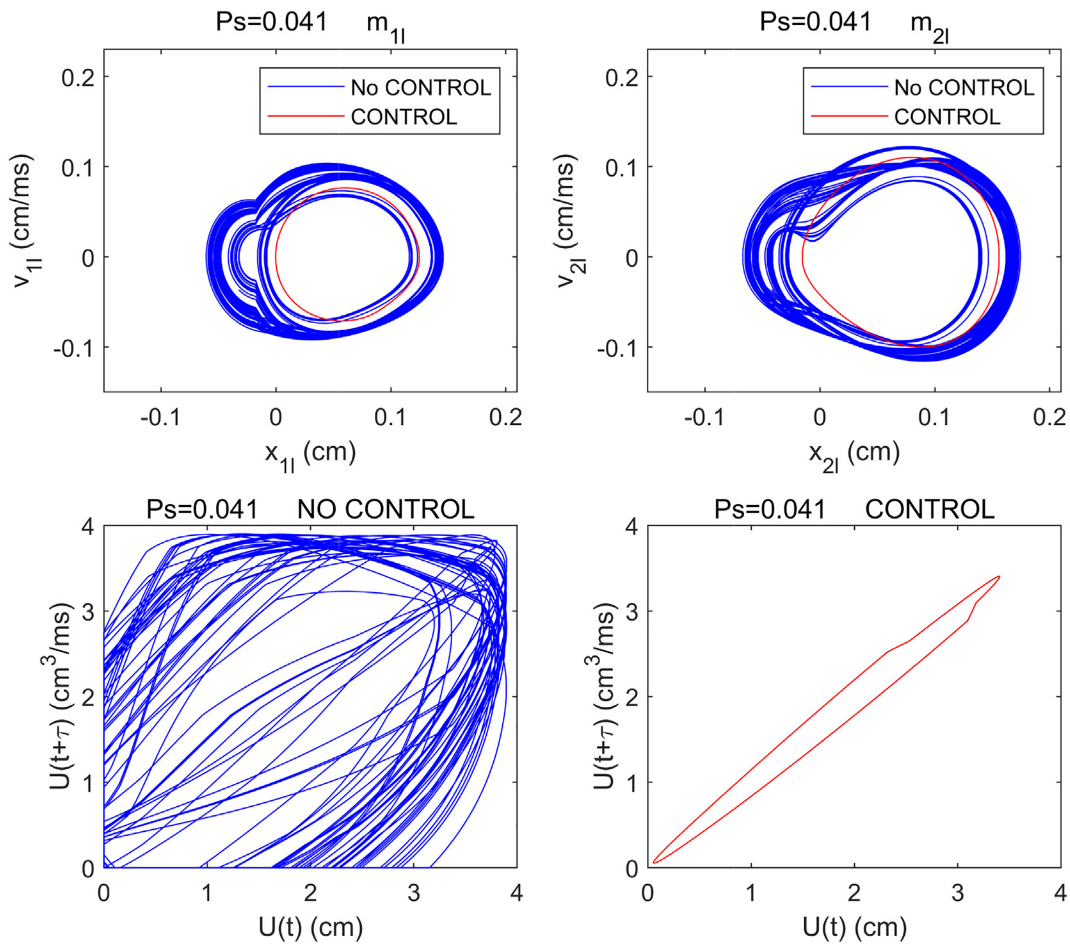

Fig. 8. First row: attractors and period-1 orbits for the system with (red) and without (blue) damping control $r_{2l\text{con}}$. Left: phase space (v_{1l}, x_{1l}), right: phase space (v_{2l}, x_{2l}). Second row: phase space plot for the glottal volume velocity $U(t+\tau)$ versus $U(t)$ without control (left) and with control (right). Results for a subglottal pressure of $P_s = 0.041$. (For interpretation of the references to colour in this figure legend, the reader is referred to the web version of this article.)

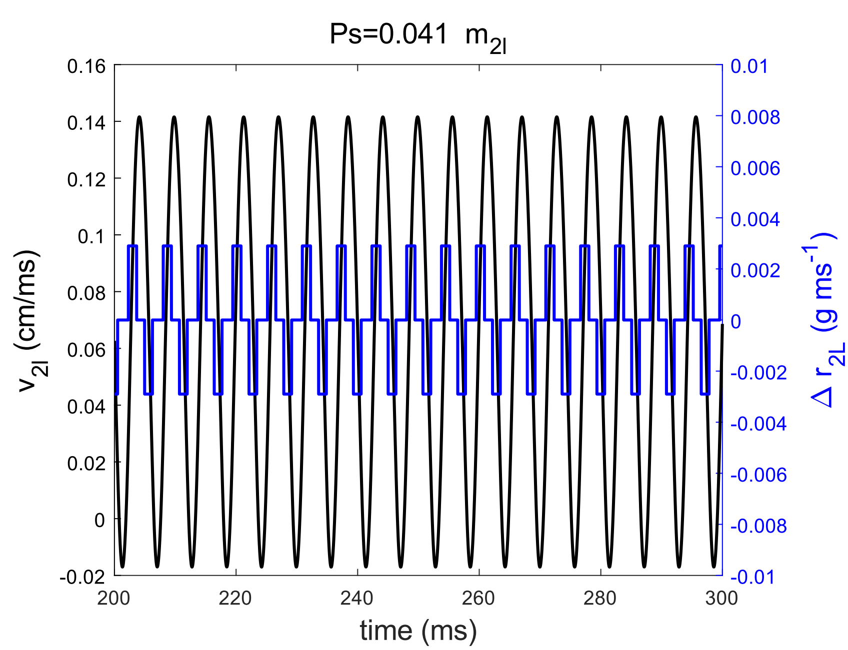

Fig. 9. Dynamic damping modification $r_{2l\text{con}}\, sgn\,(v_{2l})$ (blue line) depending on the velocity v_{2l} (black line) of the small mass m_{2l}. (For interpretation of the references to colour in this figure legend, the reader is referred to the web version of this article.)

mass velocity. Let us focus on the second mass, for which severe problems were found when just changing the value of r_{2l} to a new one. We implement the time varying damping depicted in Fig. 9, according to the general strategy in [42]. As observed in the figure, when the velocity v_{2l} augments $r_{2l\mathrm{con}}$ helps increasing the original damping r_{2l}, while it diminishes it when the opposite occurs. The effects of such variations are remarkable. Analogous results to those of Fig. 8 are plotted in Fig. 10, using the new dynamic damping law of Eq. (15). The improvement is striking. The contact between vocal folds is similar to that obtained when we acted on the first mass and U becomes totally regular again. With this approach, the average energy of the system slightly increases from $\langle E \rangle = 6.12 \times 10^{-4}$ to $\langle E_{\mathrm{con}} \rangle = 6.79 \times 10^{-4}$.

4.2.2. Damping control with volume velocity feedback for varying subglottal pressure

Up to now, the suggested damping strategies for controlling the chaotic motion of the vocal folds have been presented for a fixed value of the subglottal pressure, namely $P_s = 0.041$. However, in practice P_s will rarely be constant and can exhibit significant differences during phonation. Therefore, it would be highly recommendable to have some type of feedback mechanism that could adapt the damping of the system to subglottal pressure variations. That is the topic of this subsection.

To address the problem, we consider the subglottal pressure evolution plotted in the first row of Fig. 11. As seen, P_s is taken constant and equal to 0.041 for the first 300 ms of the simulation, and then starts growing following a parabolic profile up to a maximum of $P_{s,\,\max} = 0.08$. Once passed the maximum, the subglottal pressure diminishes and recovers its original value of $P_s = 0.041$ at $t = 1300$. In the second row of Fig. 11 we add 10% of normally distributed noise to P_s to check the robustness of the feedback strategy to be presented below.

The basic idea for controlling the vocal fold oscillations for varying P_s consists in introducing a feedback mechanism that increases or decreases the system damping depending on the effects that the evolution of P_s has on the glottal volume velocity U. We consider the following strategy for the damping of the second mass,

$$\begin{aligned}\mathbf{C} &= \mathrm{diag}(r_{1l}, r_{2l}) \to \mathbf{C} + \mathbf{C}_c \\ &= \mathrm{diag}\left(r_{1l}, r_{2l} + \left[r_{2l\mathrm{con}} + \Delta r_{2l\mathrm{con}}\left(U(t', t'' \ldots t^N)\right)\right] \mathrm{sgn}\,(v_{2l})\right).\end{aligned} \tag{16}$$

As compared to Eq. (16), at time t of the system evolution the damping value is not only modified according to the sign of the velocity v_{2l} of the second mass m_{2l}, but also by a new term, $\Delta r_{2l\mathrm{con}}(U(t', t''\ldots t^N))$, which depends on previous time values $t', t''\ldots t^N$ of the glottal volume velocity U. $\Delta r_{2l\mathrm{con}}(U(t', t''\ldots t^N))$ is computed as follows. It is first assigned a zero value. As the system evolves, every 20 ms we find the peaks of U in the preceding 30 ms and compute a linear regression for them. Usually four to five peaks are found, $U_{pk,\,i}$, $i = 1\ldots4, 5$. If the resulting slope is positive and the absolute value of the difference between the maximum and minimum peaks of U exceeds a threshold value U_{tol}=0.1, i.e. $|U_{pk,\max} - U_{pk,\min}| > U_{\mathrm{tol}}$ we take $\Delta r_{2l\mathrm{con}}(U(t', t''\ldots t^N)) = 3 \times 10^{-4}$ and the damping control increases. If $|U_{pk,\,\max} - U_{pk,\,\min}| > U_{\mathrm{tol}}$ but the slope is negative then $\Delta r_{2l\mathrm{con}}(U(t', t''\ldots t^N)) = -3 \times 10^{-4}$ and the control

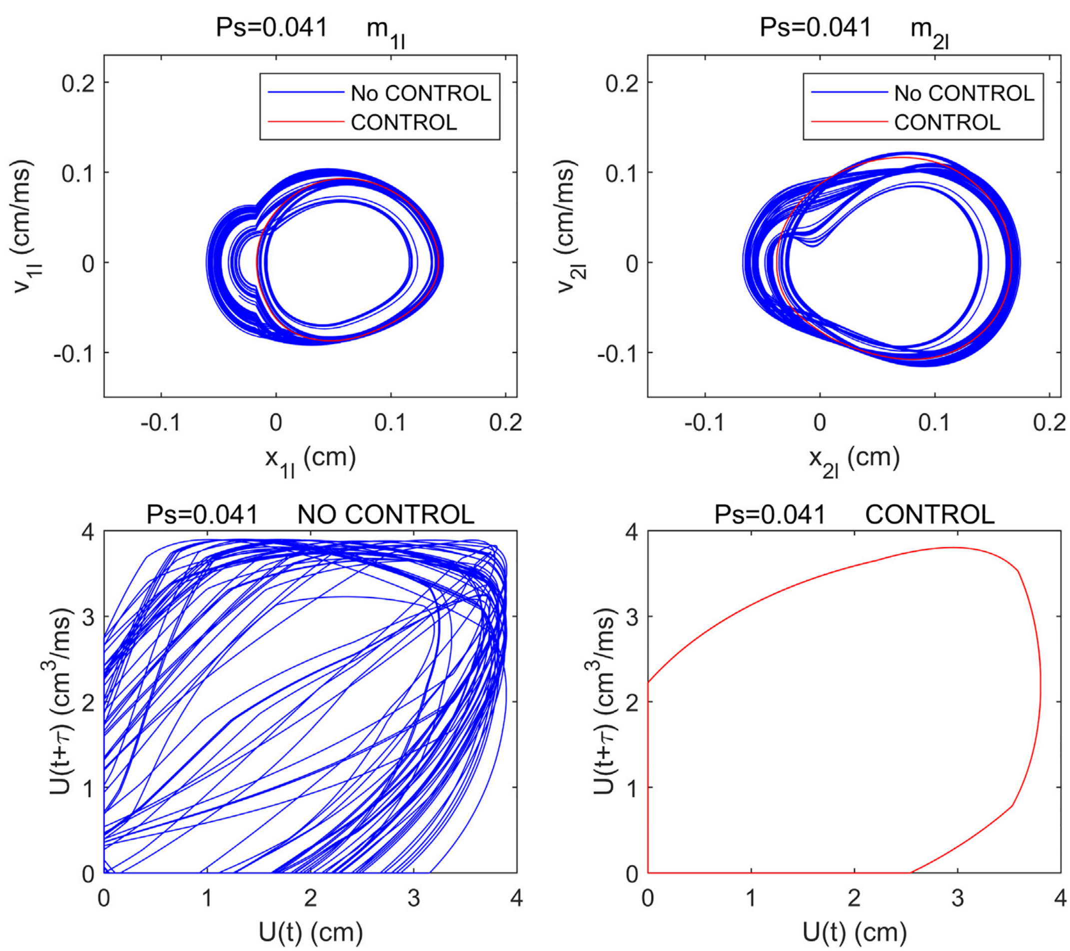

Fig. 10. First row: attractors and period-1 orbits for the system with (red) and without (blue) damping control $r_{2l} + r_{2l\mathrm{con}}\,sgn\,(v_{2l})$. Left: phase space (v_{1l}, x_{1l}), right: phase space (v_{2l}, x_{2l}). Second row: phase space plot for the glottal volume velocity $U(t+\tau)$ versus $U(t)$ without control (left) and with control (right). Results for a subglottal pressure of $P_s = 0.041$. (For interpretation of the references to colour in this figure legend, the reader is referred to the web version of this article.)

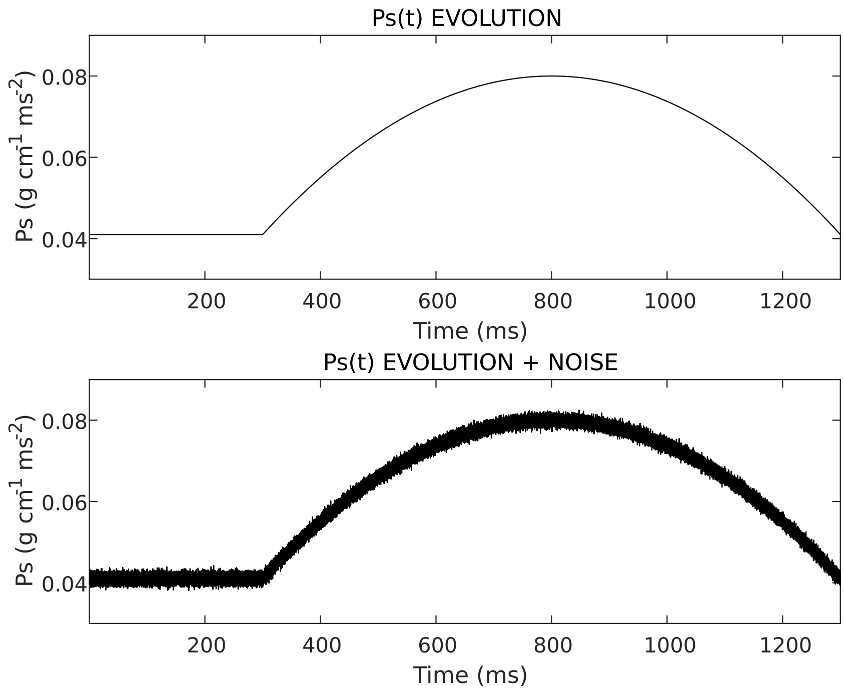

Fig. 11. Subglottal pressure evolution. Top row: P_s remains constant for the first 300 ms, then increases following a parabolic profile up to a maximum of $P_{s,\,\max} = 0.08$ and recovers its original value for $t = 1300$ ms. Bottom row: P_s exhibits the same time evolution of the top row but with a 10% of normally distributed noise.

damping diminishes. If $|U_{pk,\max} - U_{pk,\min}| < U_{\mathrm{tol}}$ no modification is made. The difference between the control damping computed according to Eq. (15) and to Eq. (16) is shown in Fig. 12. The first row in the figure presents the evolution of $r_{2l\mathrm{con}}$ sgn (v_{2l}) (blue line) and of $[r_{2l\mathrm{con}} + \Delta r_{2l\mathrm{con}}(U(t', t''\ldots t^N))]$ sgn (v_{2l}) (red line) between $t = 250$ and $t = 500$, when the subglottal pressure starts augmenting (see Fig. 11). As observed, the damping with U feedback control increases with P_s, while that without control remains unaltered. In the second row of the figure, we depict the control damping evolution between $t = 1050$ and $t = 1300$, when P_s diminishes to its original value $P_s = 0.041$. As seen in the figure, the damping with U feedback control (red line) progressively diminishes until it recovers that computed without U feedback (blue line). In the case of a more abrupt and complex time evolution of P_s than that in Fig. 11, one could think of designing alternative feedback strategies if the proposed one was not sufficient.

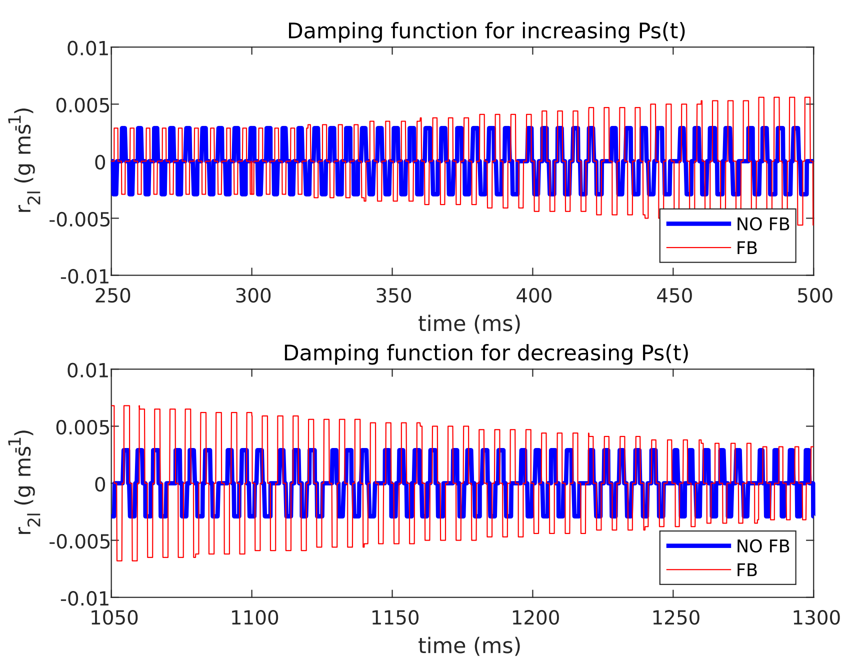

Fig. 12. Comparison between the dynamic damping control without U feedback, $r_{2l\mathrm{con}}$ sgn (v_{2l}) (blue line), and with U feedback $r_{2l\mathrm{con}} + \Delta r_{2l\mathrm{con}}(U(t', t''\ldots t^N))$ sgn (v_{2l}) (red line), when the subglottal pressure P_s starts growing according to the parabolic profile in Fig. 11 (top row), and when it gets back to its original value (bottom row). (For interpretation of the references to colour in this figure legend, the reader is referred to the web version of this article.)

The effectiveness of the U feedback damping control strategy on the vocal folds behaviour is shown in Fig. 13. The first column in the figure corresponds to the case in which no control is applied to the system. The second column contains the results for the constant damping control strategy without U feedback in Eq. (15), and the third column shows the results when the U feedback control of Eq. (16) is considered. The constant control strategy is activated for $t \geq 100$ ms and the U feedback one for $t \geq 300$ ms. As regards the row by row results in the figure, let us focus on the second row contents before commenting on the first one. The second row of the figure presents the evolution of x_{1l} with time for a total of 1300 ms, during which P_s varies according to the top row of Fig. 11. As we have decided to plot the entire time interval, individual oscillations are hardly visible. However, one can perceive from the first subfigure in the second row that the lack of control leads to strong chaotic motion, while this is slightly smoothed when applying the damping control without U feedback, and definitely turned into periodic motion when implementing the U feedback control. To better distinguish such behaviour, we have depicted three coloured stripes in the figure, green, blue and red, which respectively cover the time intervals [200,300] ms, [500,600] ms and [700,800] ms. The phase space plots (v_{1l}, x_{1l}) corresponding to these time intervals are presented in the first row of Fig. 13, using the same colour code. In

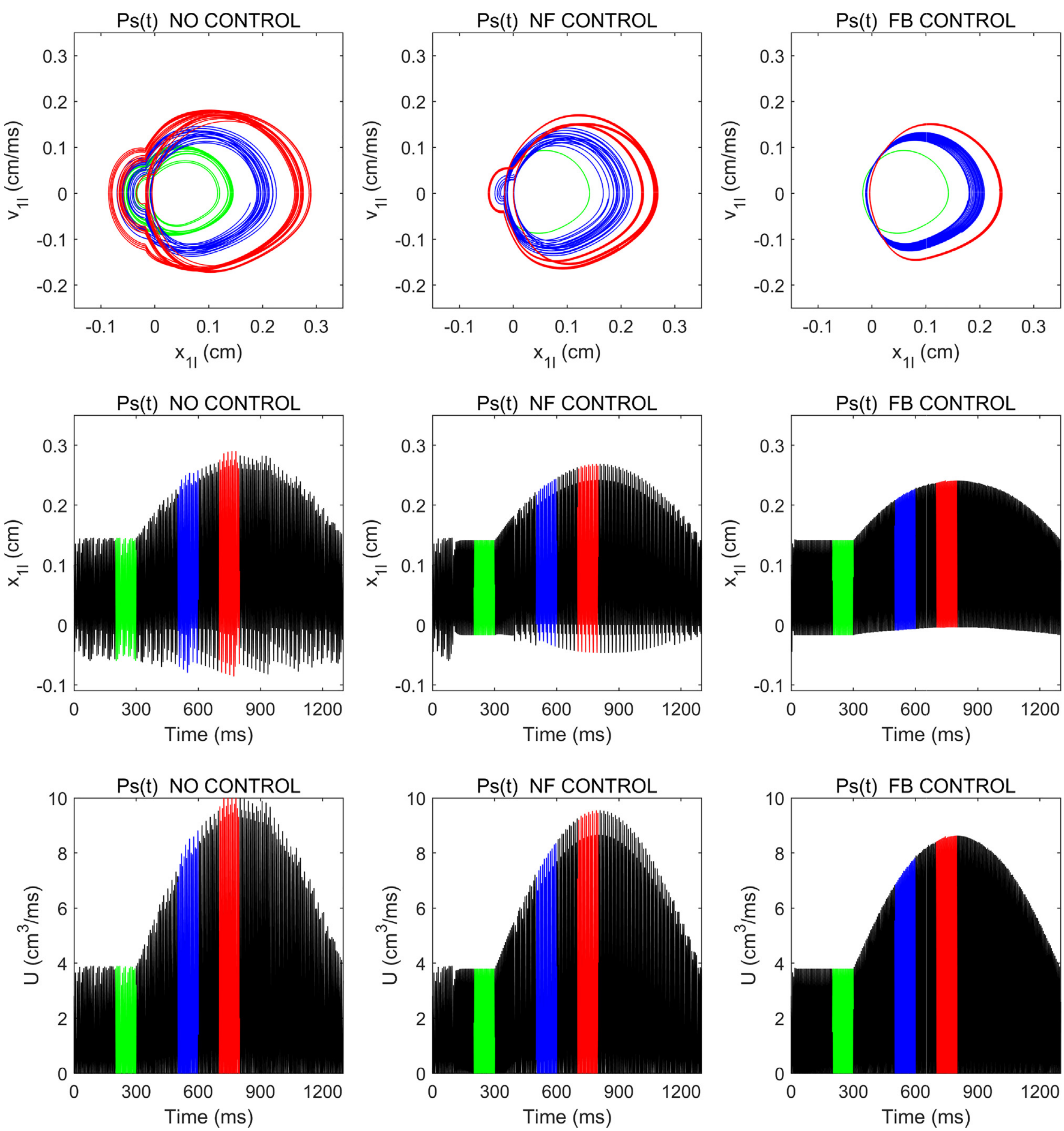

Fig. 13. Comparison of damping control strategies when P_s evolves according to the top row of Fig. 11. First column: no control. Second column: damping control in Eq. (15). Third column: damping control with U feedback in Eq. (16). The NF control is activated for $t \geq 100$ ms and the FB one for $t \geq 300$ ms. First row: phase space trajectories corresponding to the coloured time interval stripes in the second row. Second row: evolution of the first mass displacement x_{1l}. Third row: evolution of the glottal volume velocity U.

the case of no control, the trajectories evolve into strange attractors of increasing amplitude as P_s augments, as one could have expected. When applying control without U feedback, it is seen that the motion becomes periodic for [200,300] ms because for this interval the pressure still has constant value $P_s = 0.041$. Therefore a green cycle appears in the second subfigure of the first row in Fig. 13. However, as P_s gets higher, the control is insufficient and the trajectories in phase space (blue and red) soon become complex, departing from the desired periodic motion. As opposed, when the U feedback is applied, all trajectories in phase space remain periodic. The same green cycle of the previous subfigure is recovered and when the subglottal pressure is increased the motion does not loose periodicity but simply increases its amplitude (see the blue and red lines). Finally, in the third row of Fig. 13 we have plotted the time evolution of the glottal volume velocity U. The same tendencies found for x_{1l} are encountered for U, which seems to exhibit a totally regular behaviour as P_s grows if the U feedback control is activated. Given that U is the variable of primary importance in this paper, we analyse it in some more detail in Fig. 14.

The first row of Fig. 14, presents the trajectories in the phase space $\left(\dot{U}, U\right)$ for the time interval [700,800] ms (red stripe in Fig. 13) making use of Takens's theorem once more. As observed, and as already shown in previous figures, the trajectories in the case of no control are totally chaotic, which results in a very irregular pattern of U that would lead to critical problems for voice generation. When the control of Eq. (15) is applied some improvement is observed. However, the closure of the vocal folds still has very different durations (look at the zero values of the trajectories in the vertical and horizontal axes of the second subfigure in the first row). This would result again in poor voice quality. We can see, though, that the U feedback control is able to deal with the situation producing a very regular pattern for U that only presents very slight variations of the contact duration and amplitude as P_s increases. Such behaviour can also be appreciated plotting U against the position of the masses (second row of Fig. 14), x_{1l} and x_{2l}, as we did in the second row of Fig. 3. The problems detected in the phase space trajectories clearly reflect in the plots of $U(x_{1l}, x_{2l})$. It is remarkable how the U feedback control is able to stabilize the system so that $U(x_{1l}, x_{2l})$ for P_s close to 0.08 essentially exhibits the same behaviour than for $P_s = 0.021$ in Fig. 3, but with a larger amplitude.

Finally, in Fig. 15, we check whether the presented controlling mechanisms are robust with respect to noise perturbations. To that end we have applied the damping control strategy in Eq. (15) and that with U feedback in Eq. (16) to the subglottal pressure evolution in the bottom row of Fig. 11. As said, that figure corresponds to P_s in the top row but with an addition of 10% of normally distributed noise. Therefore, we want to check now if the proposed control strategies would be efficient in the demanding situation where noise is added to a varying subglottal pressure. As observed in Fig. 15, where we have plotted the same phase space plots $\left(\dot{U}, U\right)$ than in the first row of Fig. 14, both control options turn to be quite robust to the presence of noise and do not substantially alter their behaviour. Note that in the case of the U feedback control (third column in Fig. 15) the results are

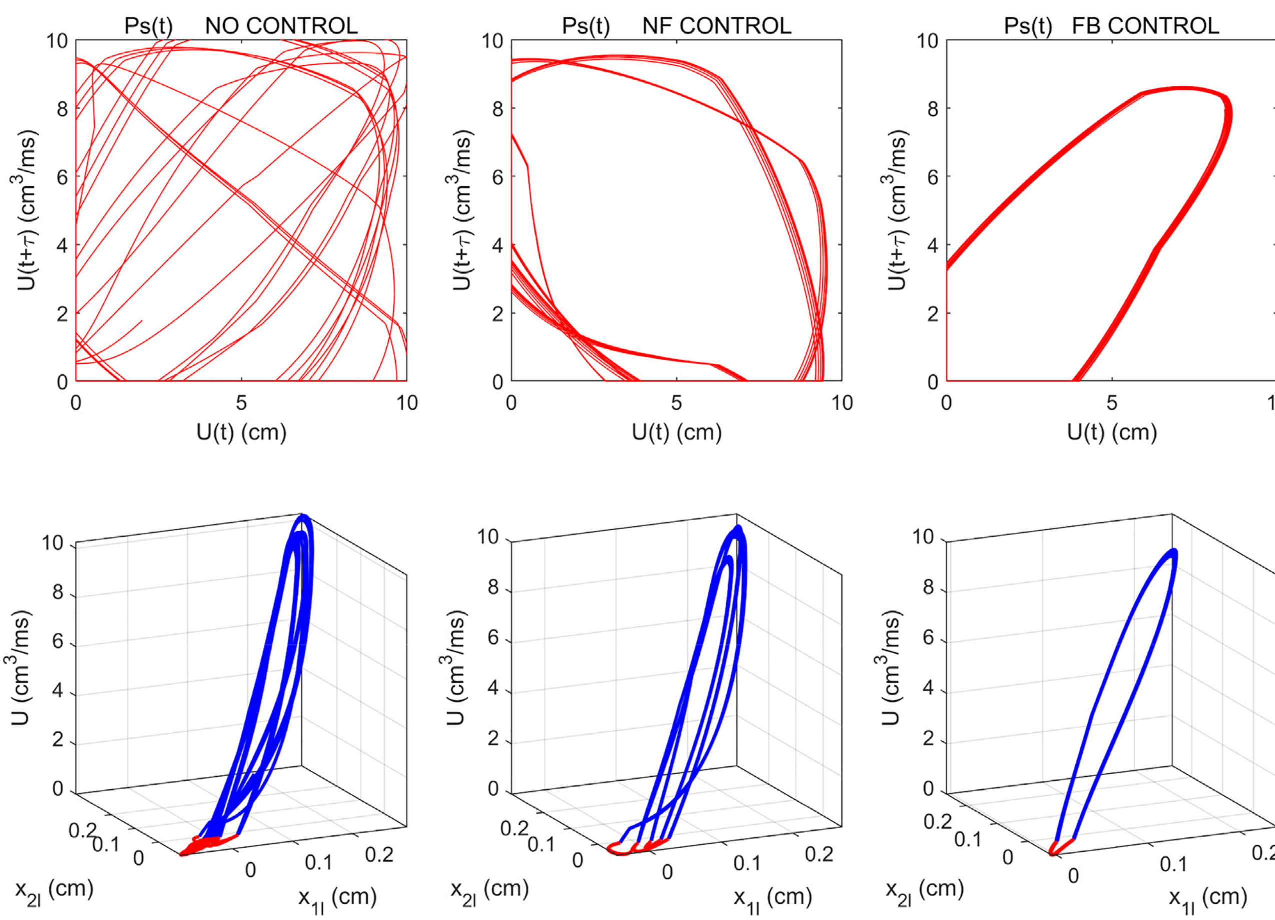

Fig. 14. First row: phase space trajectories for the glottal volume velocity $U(t+\tau)$ versus $U(t)$ in the time interval [700,800] ms (red stripe in Fig. 13) for the cases of no control, damping control for constant P_s in Eq. (15) and damping control with U feedback for varying P_s in Eq. (16). Second row: plots of $U(x_{1l}, x_{2l})$ for the same time interval. The red colour indicates zero values for U which occurs whenever the left and right masses contact. (For interpretation of the references to colour in this figure legend, the reader is referred to the web version of this article.)

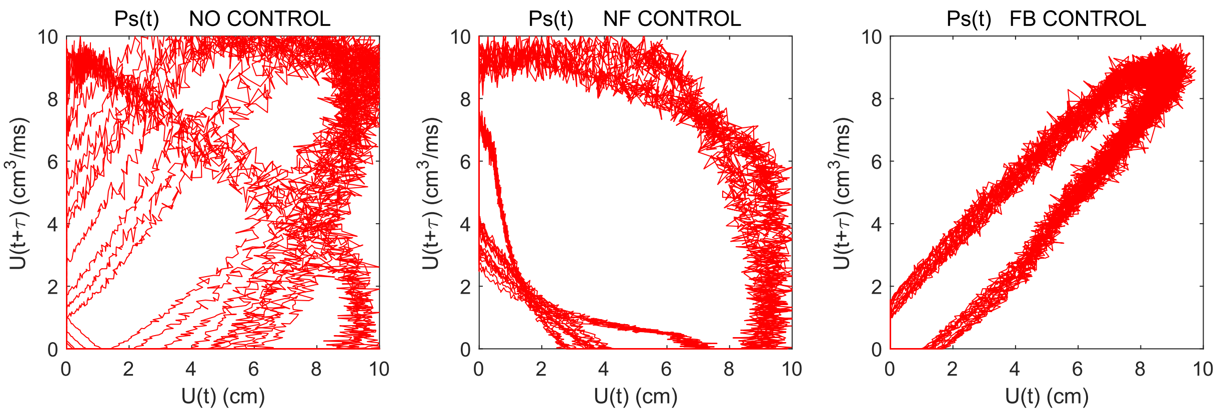

Fig. 15. Phase space trajectories for the glottal volume velocity $U(t+\tau)$ versus $U(t)$ in the time interval [700,800] ms (red stripe in Fig. 13) for the cases of no control, damping control in Eq. (15) and damping control with U feedback in Eq. (16) for varying P_s in the presence of noise (bottom row of Fig. 11). (For interpretation of the references to colour in this figure legend, the reader is referred to the web version of this article.)

quite neat and topologically resemble those in the first row, third column of Fig. 14. That could lead to admissible self-sustained oscillations of the vocal folds and proper glottal volume velocity generation as compared to control without feedback or no control at all. The robustness under noise perturbations of damping control strategies based on altering the system energy was also reported for impact problems in [43] and it is confirmed in the current example of voice phonation.

4.2.3. Stiffness control

Up to now, the chaos control strategies presented in this work have relied on modifying either the damping r_{1l} of the first mass m_{1l} or r_{2l} of m_{2l}. In this section, it will be shown that it is also possible to switch from chaotic oscillations to periodic ones by modifying the stiffness matrix of the system Eq. (4), instead of the damping one. We may consider the options of taking,

$$\mathbf{K} = \begin{pmatrix} k_{1l}+k_{cl} & -k_{cl} \\ -k_{cl} & k_{2l}+k_{cl} \end{pmatrix} \to \mathbf{K}+\mathbf{K}_c = \begin{pmatrix} k_{1l}+k_{1l\mathrm{con}}+k_{cl} & -k_{cl} \\ -k_{cl} & k_{2l}+k_{cl} \end{pmatrix} \quad (17)$$

or alternatively,

$$\mathbf{K} = \begin{pmatrix} k_{1l}+k_{cl} & -k_{cl} \\ -k_{cl} & k_{2l}+k_{cl} \end{pmatrix} \to \mathbf{K}+\mathbf{K}_c = \begin{pmatrix} k_{1l}+k_{cl} & -k_{cl} \\ -k_{cl} & k_{2l}+k_{2l\mathrm{con}}+k_{cl} \end{pmatrix}. \quad (18)$$

For the sake of brevity, and not to repeat the many tests carried out in the previous sections on damping control, we will restrain to the first option in Eq. (17) and deal with the case of constant subglottal pressure

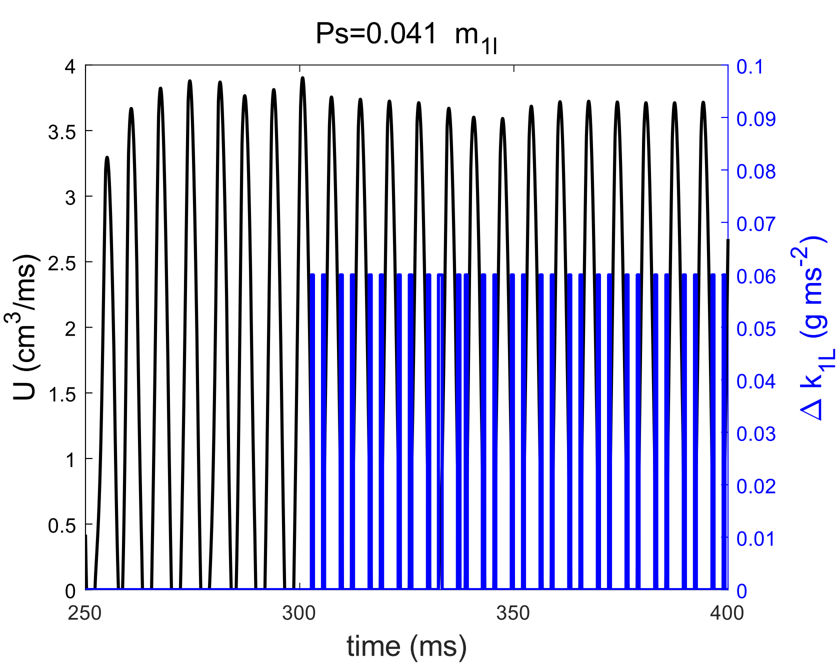

Fig. 16. Dynamic stiffness modification $\Delta k_{1l\mathrm{con}}(U(t))$ (blue line) depending on the volume velocity $U(t)$ (black line). (For interpretation of the references to colour in this figure legend, the reader is referred to the web version of this article.)

$P_s = 0.041$. In particular, we will modify the stiffness associated to the first mass in Eq. (17) according to the following law,

$$k_{1l} \to k_{1l} + \Delta k_{1l\text{con}}(U(t)). \tag{19}$$

Here, the dependence of $\Delta k_{1l\text{con}}(U(t))$ on the volume velocity U is such that if $0<U(t) \le U_{\text{tol}}$ we set $\Delta k_{1l\text{con}}(U(t)) = 0.75k_{1l}$, otherwise we set $\Delta k_{1l\text{con}}(U(t))$ to zero. A few numerical experiments have revealed that taking $U_{\text{tol}} = 1$ provides stabilization. The functioning of the stiffness control strategy is shown in Fig. 16, where the evolution of U and $\Delta k_{1l\text{con}}(U(t))$ are plotted for the interval [250,400] ms. Note that the control is activated at $t = 300$ and a few milliseconds after that, namely beyond $t = 350$, the volume velocity has already become totally regular. The efficiency of the stiffness control is more clearly shown in Fig. 17, where, as in previous figures, we compare the results for the system with (second column) and without control (first column). As clearly seen from the time evolution of x_{1l} and U (second and third rows) and the trajectories in the phase space (v_{1l}, x_{1l}) (first row), the stiffness control is totally capable to stabilize the chaotic motion. Moreover, and as in previous tests with control damping laws, in Fig. 18 we have plotted the phase space trajectories in (v_{1l}, x_{1l}) and (v_{2l}, x_{2l}) when there is no control (blue lines) and when the control is switched on (red lines). Both masses oscillate periodically. The results in the phase space $\left(\dot{U}, U\right)$ also reveal the regularity of the volume velocity which is necessary to produce a normal, healthy voice.

Finally, it is to be noted that the proposed stiffness control requires rather high values of $\Delta k_{1l\text{con}}$ (up to $0.75k_{1l}$), in comparison to the relative increase of the damping value in previous sections. As regards the system average energy, in this case it has slightly increased from $\langle E\rangle = 6.12 \times 10^{-4}$ to $\langle E_{\text{con}}\rangle = 6.44 \times 10^{-4}$.

4.2.4. Brief discussion

In the preceding sections, we have proposed several options to control the chaotic oscillations of a two-mass model of the vocal folds and recover a proper glottal pulse for voice production. It is to be mentioned that the control of non-linear oscillators has been studied in detail in the past decades (see e.g. [51,52]). The first attempts were devoted to single non-linear oscillators like the Duffing and the Van der Pol oscillators (among others), which respectively account for a cubic non-linear stiffness restoring force and a quadratic non-linear damping one. A wide range of strategies have proved useful for that purpose like the OGY

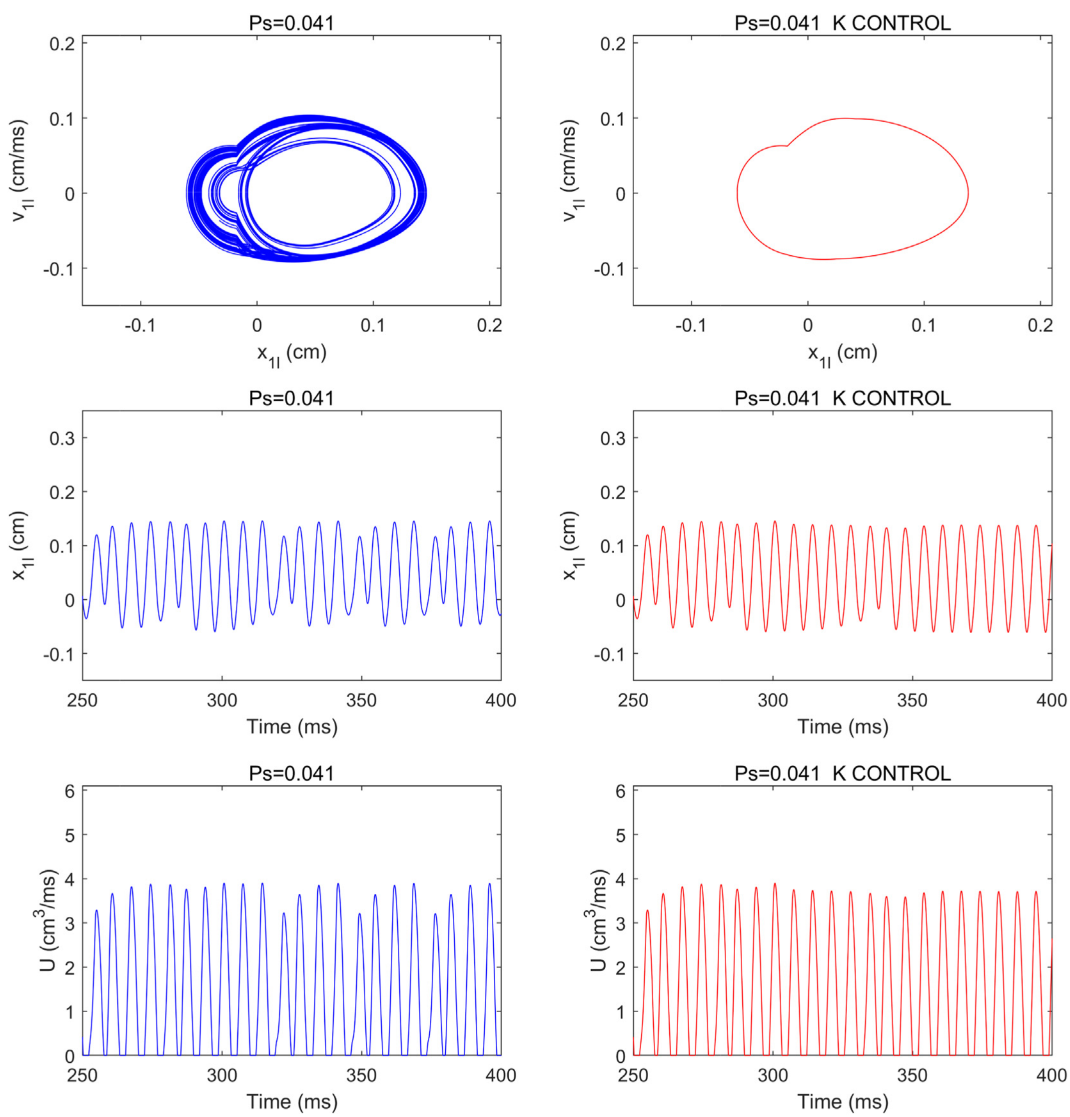

Fig. 17. Control by modifying the stiffness k_{1l} of mass m_{1l}. First column: system without control. Second column: system with stiffness control, which is activated at $t = 300$ ms. First row: phase space attractor (v_{1l}, x_{1l}). Second row: time evolution of the displacement x_{1l}. Third column: time evolution of the glottal volume flow velocity. Results for a subglottal pressure of $P_s = 0.041$.

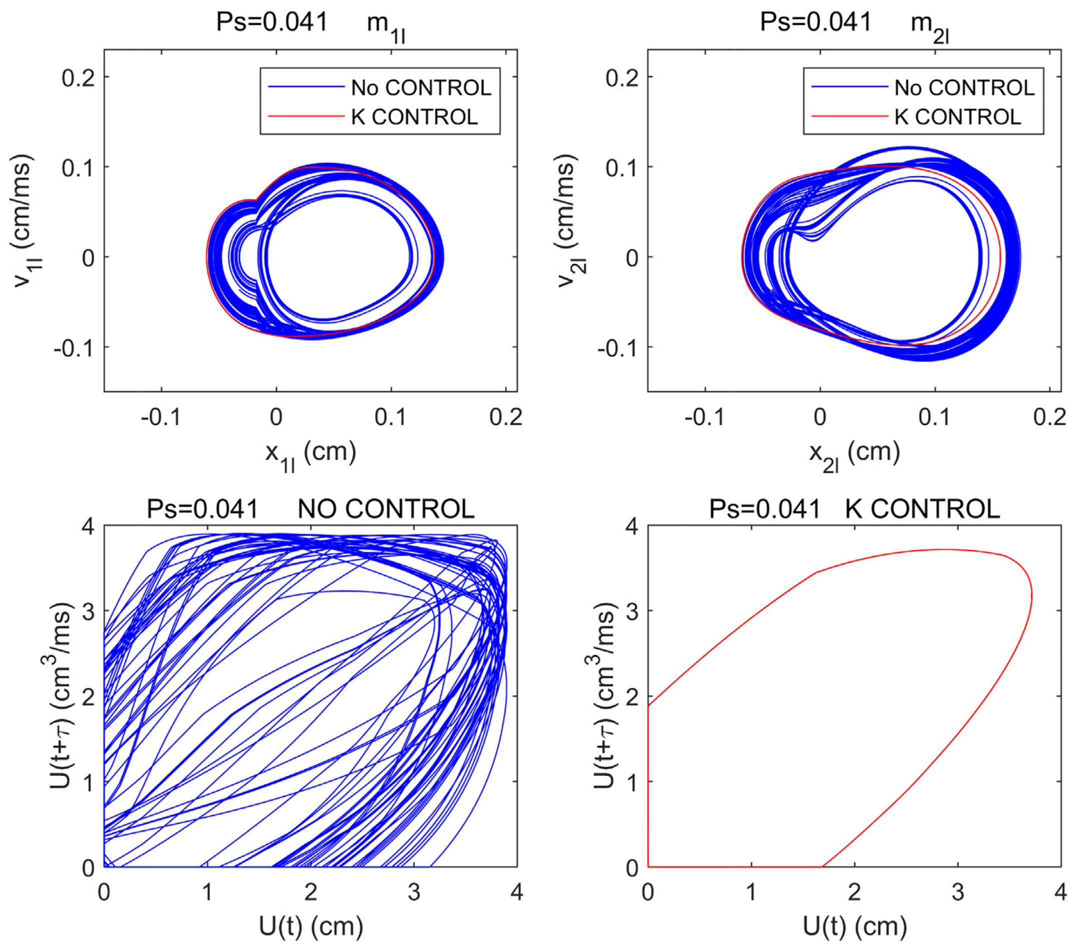

Fig. 18. First row: attractors and period-1 orbit for the system with (red) and without (blue) stiffness control $\Delta k_{1l\mathrm{con}}(U(t))$. Left: phase space (v_{1l}, x_{1l}), right: phase space (v_{2l}, x_{2l}). Second row: phase space plot for the glottal volume velocity $U(t+\tau)$ versus $U(t)$ without control (left) and with stiffness control (right). Results for a subglottal pressure of $P_s = 0.041$. (For interpretation of the references to colour in this figure legend, the reader is referred to the web version of this article.)

method [53], feedback strategies [54], non-linear adaptative approaches [55], modified linearization [56], synchronization [57], control without feedback [58], or the altering energy method [41,42] adopted in this work. As mentioned in the introduction, several of these approaches are also effective when non-linearity manifests because of impacts [37–40,43,59]. However, less articles exist on the control of systems of oscillators describing lumped physical models [40,60,61], like the one in the current work. In [41,42], it was checked that the altering energy approach is also very effective for networks of oscillators. This has been confirmed for the two-mass model in the previous sections, when applying the strategy (with variations) to distinct situations. It is expected that similar results would follow for higher dimension models of the vocal folds (e.g., that in [7]).

With the exception of the control without feedback in [58], which relies on the classical option of linking a tuned absorption damper to control the oscillator (the lack of feedback may lead to robustness problems), all other strategies in the above paragraph involve an external control force acting on the mechanical system. As this would not be possible for the vocal cords, in the previous sections we have suggested and analyzed the possibility of using ideal smart materials to control the oscillations of the vocal folds, and prevent abnormal voice production. Obviously, there is a long pathway from the theoretical analysis with ideal simple models carried out insofar to any potential real application. In addition to practical issues such as how to obtain the time series where to apply the control strategy (e.g., by means of a thin film accelerometer placed at the vocal cords), a critical aspect concerns whether smart materials exist with the capability of rapidly changing their damping and/or stiffness values at the frequencies needed for chaotic vocal folds control. This is a strong challenge for current smart materials. Besides, while a damping variation in a viscoelastic material can be frequency-dependent as either the storage modulus and the loss modulus change with the frequency of the applied load, a stiffness variation for an elastic material will mostly depend on geometry changes rather than on variations in the elastic modulus, which is an intrinsic property of the material.

From the wide range of smart materials described in the literature [44], some look promising and will be worth exploring in the future. For instance, the actuators or artificial muscles defined in [62] are a class of materials and devices that can reversibly contract, expand, or rotate as a response to an external stimulus. A recent review [63] discusses the mechanisms, limitations and challenges of several actuators including shape memory alloys, ionic-polymer/metal composites and dielectric elastomer actuators, whereas in [64] electroactivated polymers are described as actuators suitable for biomedical applications. A dynamic stimulus of the actuator, might produce a rapid damping or a stiffness variation and recent approaches to understand the mechanisms behind such behaviors have been reported in [65,66].

5. Conclusions

In this paper we have suggested the idea of a voice pacemaker that could control chaotic oscillations of the vocal folds and revert them to periodic ones. That pacemaker could be built by attaching a smart material to the vocal cords, with the capability of having tunable time varying damping and stiffness values. For simplicity, the mass of the smart material has been assumed negligible as compared to those of the vocal folds. Simulations have been performed for a symmetric two-mass model in which oscillations become chaotic for excessive subglottal pressure.

In the two-mass model, each vocal cord is characterized by two masses, the lower one being twenty times bigger than the upper one. To begin with, it has been shown that, for a fixed value of the subglottal pressure, an effective control strategy based on altering the system energy consists in slightly diminish the damping of the biggest mass through the action of the smart material. This stabilizes the motion of the vocal folds, which becomes periodic and closes the glottis at regular time intervals. That can be clearly seen in phase space plots of the motion of the masses, as well as when applying Taken's theorem to visualize the glottal volume velocity in phase space. Remember that a regular glottal volume velocity pulse is the key for proper voice generation. The situation is more intricate if one attempts to control the upper mass of the vocal cords because reducing its damping does not suffice. The vocal fold oscillations can become periodic but they do not collide, i.e., the glottis does not close. This would lead to an undesirable breathy glottal volume velocity and abnormal voice production. A more complex damping law is therefore required to get an admissible glottal pulse if one wants to control the system through the upper mass instead of the lower one. The trick here is to supply additional damping depending on the sign of the velocity of the upper mass. In this way, one can recover a similar control to that achieved with the first mass.

On the other hand, in a realistic situation the subglottal pressure will be rarely constant but vary with time. It would be thus interesting to establish a feedback control strategy to deal with that circumstance. This has been done for the very demanding case of controlling the upper mass. For varying subglottal pressure, we do not only change the sign of the damping depending on the upper mass velocity but we also modify its amplitude depending on previous values of the glottal volume velocity. Again, the results have clearly shown the validity of this strategy and how periodicity is recovered yielding a regular glottal pulse for correct voice generation. Another interesting aspect is that in practice, the subglottal pressure will not only evolve with time but present noise perturbations. The feedback control has been also tested in such condition by adding a 10% of normally distributed noise to the subglottal pressure signal. It has been shown that the feedback control is noticeably robust to the presence of noise and that the resulting glottal pulses present admissible variations in amplitude and in the glottis closure time.

To finish the paper, we have considered the option of controlling the chaotic motion of the vocal folds by acting on the stiffness of the smart material instead of acting on its damping. For constant subglottal pressure, it has been proposed to modify the stiffness of the lower mass of the vocal folds depending on the value of the glottal volume velocity. If that exceeds a given tolerance value, the stiffness augments by a constant factor, while no change is made for smaller values than the threshold. Once more, time evolution and phase space plots for the mass motion and volume velocity have revealed the efficiency of the method. Therefore, stiffness control could be also an option and in future works it will be worth exploring whether it may be also reliable for varying and/or noisy subglottal pressure.

The work presented in this paper intends to open the door to new ways of dealing with pathological voice disorders. It is to be mentioned though, that our analysis has been carried out for a very simple two-mass model of the vocal folds. In forthcoming works, we will analyse the smart material control approach for models involving lateral paralyses and polyps which break the symmetry of the current model and also introduce new types of non-linearities. It is expected that the type of chaos control strategy presented herein could well adapt to those more complex models and situations.

CRediT authorship contribution statement

Oriol Guasch: Conceptualization, Methodology, Software, Visualization, Formal analysis, Investigation, Validation, Writing - Original Draft, Review & Editing.

Annemie Van Hirtum: Formal analysis, Investigation, Validation, Review & Editing.

A. Inés Fernández: Formal analysis, Investigation, Validation, Review & Editing.

Marc Arnela: Formal analysis, Investigation, Validation, Review & Editing.

Declaration of competing interest

The authors declare that they have no known competing financial interests or personal relationships that could have appeared to influence the work reported in this paper.

Acknowledgements

The first and fourth authors thank the support of the project FEMVoQ (PID2020-120441GB-I00-AEI-10.13039/501100011033) from the Spanish Ministerio de Ciencia e Innovación. The second author would like to acknowledge the Full3DTalkingHead project (ANR-20-CE23-0008-03) from l'Agence Nationale de la Recherche. The third author would like to thank the Catalan Government for the quality accreditation given to her research group DIOPMA (2017 SGR 0118). DIOPMA is certified agent TECNIO in the category of technology developers from the Government of Catalonia.

References

[1] Van den Berg J. Myoelastic-aerodynamic theory of voice production. J Speech Hear Res. 1958;1:227–44.
[2] Titze I. The myoelastic aerodynamic theory of phonation. Iowa City: National Centre for Voice and Speech; 2006..
[3] Ishizaka K, Flanagan J. Synthesis of voiced sounds from a two-mass model of the vocal cords. Bell Syst Tech J. 1972;51:1233–68.
[4] Lucero JC. Dynamics of the two-mass model of the vocal folds: equilibria, bifurcations, and oscillation region. J Acoust Soc Am. 1993;94:3104–11.
[5] Steinecke I, Herzel H. Bifurcations in an asymmetric vocal-fold model. J Acoust Soc Am. 1995;97:1874–84.
[6] Sommer DE, Erath BD, Zanartu M, Peterson SD. Corrected contact dynamics for the Steinecke and Herzel asymmetric two-mass model of the vocal folds. J Acoust Soc Am. 2012;132:EL271–6.
[7] Story BH, Titze IR. Voice simulation with a body-cover model of the vocal folds. J Acoust Soc Am. 1995;97:1249–60.
[8] Laje R, Gardner T, Mindlin G. Continuous model for vocal fold oscillations to study the effect of feedback. Phys Rev E. 2001;64:056201.
[9] Zhang Y, Jiang JJ. Chaotic vibrations of a vocal fold model with a unilateral polyp. J Acoust Soc Am. 2004;115:1266–9.
[10] Erath BD, Zanartu M, Stewart KC, Plesniak MW, Sommer DE, Peterson SD. A review of lumped-element models of voiced speech. Speech Commun. 2013;55:667–90.
[11] Cisonni J, Van Hirtum A, Pelorson X, Lucero J. The influence of geometrical and mechanical input parameters on theoretical models of phonation. Acta Acust United Acust. 2011;97:291–302.
[12] Luizard P, Pelorson X. Threshold of oscillation of a vocal fold replica with unilateral surface growths. J Acoust Soc Am. 2017;141:3050–8.
[13] Fatehi Nia M, Akrami MH. Bifurcation and chaos in a one mass discrete time vocal fold dynamical model. Int J Nonlinear Anal Appl. 2021;12:305–15.
[14] Cisonni J, Van Hirtum A, Pelorson X, Willems J. Theoretical simulation and experimental validation of inverse quasi-one-dimensional steady and unsteady glottal flow models. J Acoust Soc Am. 2008;124:535–45.
[15] Mittal R, Erath BD, Plesniak MW. Fluid dynamics of human phonation and speech. Annu Rev Fluid Mech. 2013;45:437–67.
[16] Leonov GA, Kuznetsov NV. Hidden attractors in dynamical systems. From hidden oscillations in Hilbert–Kolmogorov, Aizerman, and Kalman problems to hidden chaotic attractor in chua circuits. Int J Bifurc Chaos. 2013;23:1330002.
[17] Wei Z, Zhang W, Wang Z, Yao M. Hidden attractors and dynamical behaviors in an extended rikitake system. Int J Bifurc Chaos. 2015;25:1550028.
[18] Wei Z, Zhang W, Yao M. On the periodic orbit bifurcating from one single non-hyperbolic equilibrium in a chaotic jerk system. Nonlinear Dyn. 2015;82:1251–8.
[19] Wei Z, Moroz I, Sprott JC, Wang Z, Zhang W. Detecting hidden chaotic regions and complex dynamics in the self-exciting homopolar disc dynamo. Int J Bifurc Chaos. 2017;27:1730008.
[20] Wei Z, Zhang W. Hidden hyperchaotic attractors in a modified lorenz–stenflo system with only one stable equilibrium. Int J Bifurc Chaos. 2014;24:1450127.
[21] Wei Z, Yu P, Zhang W, Yao M. Study of hidden attractors, multiple limit cycles from hopf bifurcation and boundedness of motion in the generalized hyperchaotic rabinovich system. Nonlinear Dyn. 2015;82:131–41.
[22] Wei Z, Moroz I, Sprott J, Akgul A, Zhang W. Hidden hyperchaos and electronic circuit application in a 5d self-exciting homopolar disc dynamo. Chaos. 2017;27:033101.

[23] Broniatowski M, Kaneko S, Jacobs G, Nose Y, Tucker HM. Laryngeal pacemaker. Part II. Electronic pacing of reinnervated posterior cricoarytenoid muscles in the canine. Laryngoscope. 1985;95:1194–8.
[24] Broniatowski M, Tucker HM, Kaneko S, Jacobs G, Nose Y. Laryngeal pacemaker. Part I. Electronic pacing of reinnervated strap muscles in the dog. Otolaryngol Head Neck Surg. 1986;94:41–4.
[25] Goldfarb D, Keane WM, Lowry LD. Laryngeal pacing as a treatment for vocal fold paralysis. J Voice. 1994;8:179–85.
[26] Zealear DL, Billante CR, Courey MS, Netterville JL, Paniello RC, Sanders I, Herzon GD, Goding GS, Mann W, Ejnell H, et al. Reanimation of the paralyzed human larynx with an implantable electrical stimulation device. Laryngoscope. 2003;113:1149–56.
[27] Mueller AH, Hagen R, Foerster G, Grossmann W, Baumbusch K, Pototschnig C. Laryngeal pacing via an implantable stimulator for the rehabilitation of subjects suffering from bilateral vocal fold paralysis: a prospective first-in-human study. Laryngoscope. 2016;126:1810–6.
[28] Mueller AH. Laryngeal pacing. Neurolaryngology. Springer; 2018. p. 173–83.
[29] Jiang JJ, Zhang Y, Stern J. Modeling of chaotic vibrations in symmetric vocal folds. J Acoust Soc Am. 2001;110:2120–8.
[30] Ott E, Grebogi C, Yorke JA. Controlling chaos. Phys Rev Lett. 1990;64:1196.
[31] de Souza SL, Caldas IL. Controlling chaotic orbits in mechanical systems with impacts. chaos solitFractals. 2004;19:171–8.
[32] Pyragas K. Continuous control of chaos by self-controlling feedback. Phys Lett A. 1992;170:421–8.
[33] Pyragas K, Tamaševičius A. Experimental control of chaos by delayed self-controlling feedback. Phys Lett A. 1993;180:99–102.
[34] Boccaletti S, Grebogi C, Lai Y-C, Mancini H, Maza D. The control of chaos: theory and applications. Phys Rep. 2000;329:103–97.
[35] Pyragas K. Delayed feedback control of chaos. Philos Trans R SocA. 2006;364: 2309–34.
[36] Wernecke H, Sándor B, Gros C. Chaos in time delay systems, an educational review. Phys Rep. 2019;824:1–40.
[37] De Souza S, Caldas I, Viana R, Balthazar JM, Brasil R. Impact dampers for controlling chaos in systems with limited power supply. J Sound Vib. 2005;279:955–67.
[38] Lee J-Y, Yan J-J. Control of impact oscillator. chaos solitFractals. 2006;28:136–42.
[39] De Souza SL, Caldas IL, Viana RL, Balthazar JM. Control and chaos for vibro-impact and non-ideal oscillators. J Theor Appl Mech. 2008;46:641–64.
[40] Luo G, Lv X. Controlling bifurcation and chaos of a plastic impact oscillator. Nonlinear Anal Real World Appl. 2009;10:2047–61.
[41] Tereshko V, Chacón R, Preciado V. Controlling chaotic oscillators by altering their energy. Phys Lett A. 2004;320:408–16.
[42] Tereshko V. Control and identification of chaotic systems by altering their energy. chaos solitFractals. 2009;40:2430–46.
[43] de Souza SL, Caldas IL, Viana RL. Damping control law for a chaotic impact oscillator. chaos solitFractals. 2007;32:745–50.
[44] Hassani FA, Shi Q, Wen F, He T, Haroun A, Yang Y, et al. Smart materials for smart healthcare–moving from sensors and actuators to self-sustained nanoenergy nanosystems. Smart Mat Med. 2020;1:92–124.
[45] Arnela M, Guasch O, Alías F. Effects of head geometry simplifications on acoustic radiation of vowel sounds based on time-domain finite-element simulations. J Acoust Soc Am. 2013;134(4):2946–54.
[46] Arnela M, Dabbaghchian S, Blandin R, Guasch O, Engwall O, Van Hirtum A, Pelorson X. Influence of vocal tract geometry simplifications on the numerical simulation of vowel sounds. J Acoust Soc Am. 2016;140:1707–18.
[47] Guasch O, Arnela M, Codina R, Espinoza H. A stabilized finite element method for the mixed wave equation in an ALE framework with application to diphthong production. Acta Acust United Acust. 2016;102:94–106.
[48] Dabbaghchian S, Arnela M, Engwall O, Guasch O. Simulation of vowel-vowel utterances using a 3D biomechanical-acoustic model. Int J Numer Methods Biomed Eng. 2021;37:e3407.
[49] Fraser AM, Swinney HL. Independent coordinates for strange attractors from mutual information. Phys Rev A. 1986;33:1134.
[50] Van Hirtum A, Bouvet A, Pelorson X. Quantifying the auto-oscillation complexity following water spraying with interest for phonation. Phys Rev E. 2019;100:043111.
[51] Blazéjczyk B, Kapitaniak T, Wojewoda J, Brindley J. Controlling chaos in mechanical systems. Appl Mech Rev. 1993;46:385–91.
[52] Lakshmanan M, Murali K. Chaos in nonlinear oscillators: controlling and synchronization. World Scientific. 1996.;13.
[53] Akhmet M, Fen M. Chaotic period-doubling and ogy control for the forced duffing equation. Commun Nonlinear Sci Numer Simul. 2012;17:1929–46.
[54] Ma S, Lu Q, Feng Z. Double hopf bifurcation for van der pol-duffing oscillator with parametric delay feedback control. J Math Anal Appl. 2008;338:993–1007.
[55] Cao Y. A nonlinear adaptive approach to controlling chaotic oscillators. Phys Lett A. 2000;270:171–6.
[56] Chen L-Q, Liu Y-Z. A modified exact linearization control for chaotic oscillators. Nonlinear Dyn. 1999;20:309–17.
[57] Astakhov V, Anishchenko V, Kapitaniak T, Shabunin A. Synchronization of chaotic oscillators by periodic parametric perturbations. Phys D. 1997;109:11–6.
[58] Kapitaniak T. Controlling chaotic oscillators without feedback. chaos solitFractals. 1992;2:519–30.
[59] Lin R, Ewins D. Chaotic vibration of mechanical systems with backlash. Mech Syst Signal Process. 1993;7:257–72.
[60] Sepulchre J, Babloyantz A. Controlling chaos in a network of oscillators. Phys Rev E. 1993;48:945.
[61] Xiang L, Jia Y, Hu A. Bifurcation and chaos analysis for multi-freedom gear-bearing system with time-varying stiffness. App Math Model. 2016;40:10506–20.
[62] Mirvakili SM, Pazukha A, Sikkema W, Sinclair CW, Spinks GM, Baughman RH, Madden JD. Niobium nanowire yarns and their application as artificial muscles. Adv Funct Mater. 2013;23:4311–6.
[63] Mirvakili SM, Hunter IW. Artificial muscles: mechanisms, applications, and challenges. Acta Math. 2018;30:1704407.
[64] Q. Zhang C. Huang F. Xia J. Su n.d. Electric EAP, in Electroactive polymer (EAP) actuators as artificial muscles: reality, potential, and challenges, Y. Bar-Cohen (Ed.), SPIE press, pp. 95–148.
[65] Giovinco V, Kotak P, Cichella V, Maletta C, Lamuta C. Dynamic model for the tensile actuation of thermally and electro-thermally actuated twisted and coiled artificial muscles (TCAMs). Smart Mater Struct. 2019;29:025004.
[66] Y. Yang Z. Kan Y. Zhang Y. A. Tse M. Y. Wang n.d. A novel variable stiffness actuator based on pneumatic actuation and supercoiled polymer artificial muscles, in: 2019 international conference on robotics and automation (ICRA), IEEE, pp. 3983–3989.